frontiers in Earth Science

ORIGINAL RESEARCH
published: 03 January 2022
doi: 10.3389/feart.2021.785659

Sedimentary and Source-to-Sink Evolution of Intracontinental Basins: Implications for tectonic and Climate Evolution in the Late Mesozoic (Southern Junggar Basin, NW China)

Xutong Guan[1], Chaodong Wu[1], Xuecai Zhang[2], Weiwei Jia[3] and Wei Zhang[1]*

[1]Key Laboratory of Orogenic Belts and Crustal Evolution, Ministry of Education, School of Earth and Space Sciences, Peking University, Beijing, China, [2]Petroleum Exploration Management Center of Shengli Oilfield Company of SINOPEC, Dongying, China, [3]Geologic Party No.216, China National Nuclear Corporation, Urumqi, China

Sedimentary investigations, petrography, heavy mineral and conglomerate component analyses, and detrital zircon U-Pb geochronology were conducted to reconstruct the sedimentary and source-to-sink evolution of the Southern Junggar Basin, an intracontinental basin in the late Mesozoic. A paludal deltaic environment evolved into a fluvial environment, and abruptly prograded into alluvial fan and aeolian environments in the Late Jurassic, which was replaced by fan deltaic and lacustrine environments in the Early Cretaceous. Three source-to-sink systems were identified, according to different source-to-sink system features. In the northern piedmont of the Tianshan Orogenic Belt, the North Tianshan Orogenic Belt mainly provided sediments in the Late Jurassic. The North Tianshan and Central Tianshan Orogenic Belt both supplied sediments in the Early Cretaceous. In the northern piedmont of the Bogda Orogenic Belt, the Bogda Orogenic Belt was constantly the primary provenance, and the Tianshan Orogenic Belt also provided sediments. Sediment recycling occurred in the basin margin in the Late Jurassic and more metamorphic rocks were denudated in the Early Cretaceous. The source-to-sink system shrank in the Late Jurassic and expanded in the Early Cretaceous. This source-to-sink evolution and the conglomerates in the Kalazha Formation with seismite structures responded to the aridification in the Late Jurassic, the uplift of the Bogda and Tianshan Orogenic Belts in the Late Jurassic, and the exhumation of the Bogda and Tianshan Orogenic Belts in the Early Cretaceous.

Keywords: sediment recycling process, seismite, Kalazha conglomerate, Bogda Orogenic Belt, Tianshan Orogenic Belt

OPEN ACCESS

Edited by:
Xiubin Lin,
Zhejiang University, China

Reviewed by:
Bin Deng,
Chengdu University of Technology, China
Xianyan Wang,
Nanjing University, China

****Correspondence:***
Chaodong Wu
cdwu@pku.edu.cn

Specialty section:
This article was submitted to Structural Geology and Tectonics, a section of the journal Frontiers in Earth Science

Received: *29 September 2021*
Accepted: *22 November 2021*
Published: *03 January 2022*

Citation:
Guan X, Wu C, Zhang X, Jia W and Zhang W (2022) Sedimentary and Source-to-Sink Evolution of Intracontinental Basins: Implications for tectonic and Climate Evolution in the Late Mesozoic (Southern Junggar Basin, NW China). Front. Earth Sci. 9:785659. doi: 10.3389/feart.2021.785659

INTRODUCTION

The source-to-sink approach focuses on the connection and reconstruction of the various components of siliciclastic sedimentary systems from initial source areas through the dispersal system to catchment areas, and it has more recently been applied to deep-time stratigraphic systems (Bhattacharya et al., 2016; Walsh et al., 2016). Source-to-sink systems of intracontinental basins are different from source-to-sink systems of continental margins, which are not influenced by the sea

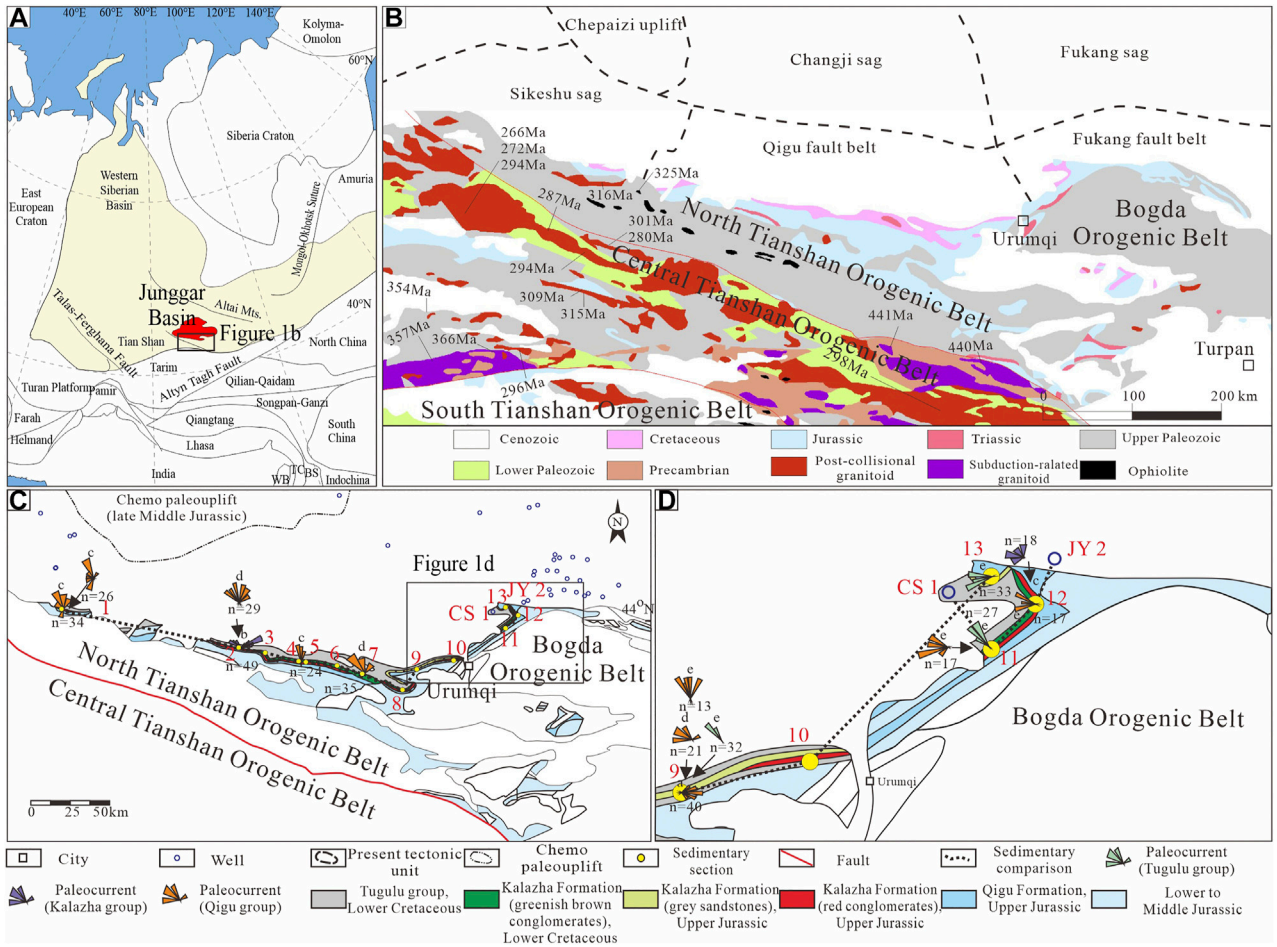

FIGURE 1 | (A) Simplified tectonic map of Asia, modified from Ma (2002). The light yellow area shows the location of the Central Asia Orogenic Belt. BS-Baoshan Block; TC-Tengchong Block; WB-West Burma Block; **(B)** geological map of the Tianshan and Bogda Orogenic Belts. The age data are provided in Supplementary Material S2 **(C, D)** stratigraphic distribution and paleocurrents of the Upper Jurassic and Lower Cretaceous in the southern Junggar Basin. 1. Sikeshu section; 2. Manasi section; 3. Qingshuihe River section; 4. Taxihe River section; 5. Queergou section; 6. Hutubi River section; 7. Jiangong mine section; 8. Dongwozi section; 9. Toutunhe River section; 10. Wangjiagou section; 11. Baiyanggou section; 12. Shuimohe section; 13. Dahongshan section. The paleocurrents are from the following sources: a. Fang et al., 2019; b. Hendrix et al., 1992; c. Zhou, 2020; d. Zhou et al., 2019; and e. Wang et al., 2007. The Upper Jurassic to Lower Cretaceous strata thickness is exaggerated for several kilometers to better show the stratigraphic distribution. The boundaries of paleouplift in the late Middle Jurassic refers to He et al. (2008).

and mainly exhibit terrestrial deposits. Intracontinental basins have been termed "Chinese-type basins", "collisional successor basins", "walled basins", and "plate interior polyphase basins" (Bally and Snelson, 1980; Graham et al., 1993; Carroll et al., 2010; Johnson and Ritts, 2012) and are typical in western China (e.g., the Junggar Basin, Tarim Basin, Qaidam Basin, and Sichuan Basin). These intracontinental basins are relatively undeformed within the basin interiors yet significantly deformed at or near the basin margins (e.g., Graham et al., 1993; Ritts et al., 2009; Liu et al., 2012). They also typically record polyphase deformation and are abundant in coal, petroleum, and evaporite minerals. Understanding the source-to-sink systems in these intracontinental basins has important implications for unraveling their basin and orogenic evolution.

Aridification happened in the Late Jurassic in Central and East Asia, which covered over an area of ~$1*10^7$ km^2 (Yi et al., 2019). The Tianshan and Bogda Orogenic Belts are assumed to have experienced uplift in the Late Jurassic, as suggested by a cooling event based on apatite fission-track data (Dumitru, et al., 2001; Guo et al., 2006; Shen et al., 2006, 2008; Tang et al., 2015). Located in the southern Central Asia Orogenic Belt (**Figure 1A**), the southern Junggar Basin (SJB) is in the northern piedmont of the Tianshan and Bogda Orogenic Belts and has been an intracontinental basin since the Permian. The basin infilling in the SJB in the Late Mesozoic recorded the aridification and the intracontinental mountain building of the Tianshan and Bogda Orogenic Belts. The coal-bearing strata evolved into red beds in the Late Jurassic. Red fine-grained deposits transitioned into tens of meters-thick conglomerate successions (Kalazha Formation) in the latest Jurassic that underlaid gray or greenish fine-grained deposits in the Lower Cretaceous. Jolivet et al. (2017) believed that the conglomerates in the latest Jurassic were largely

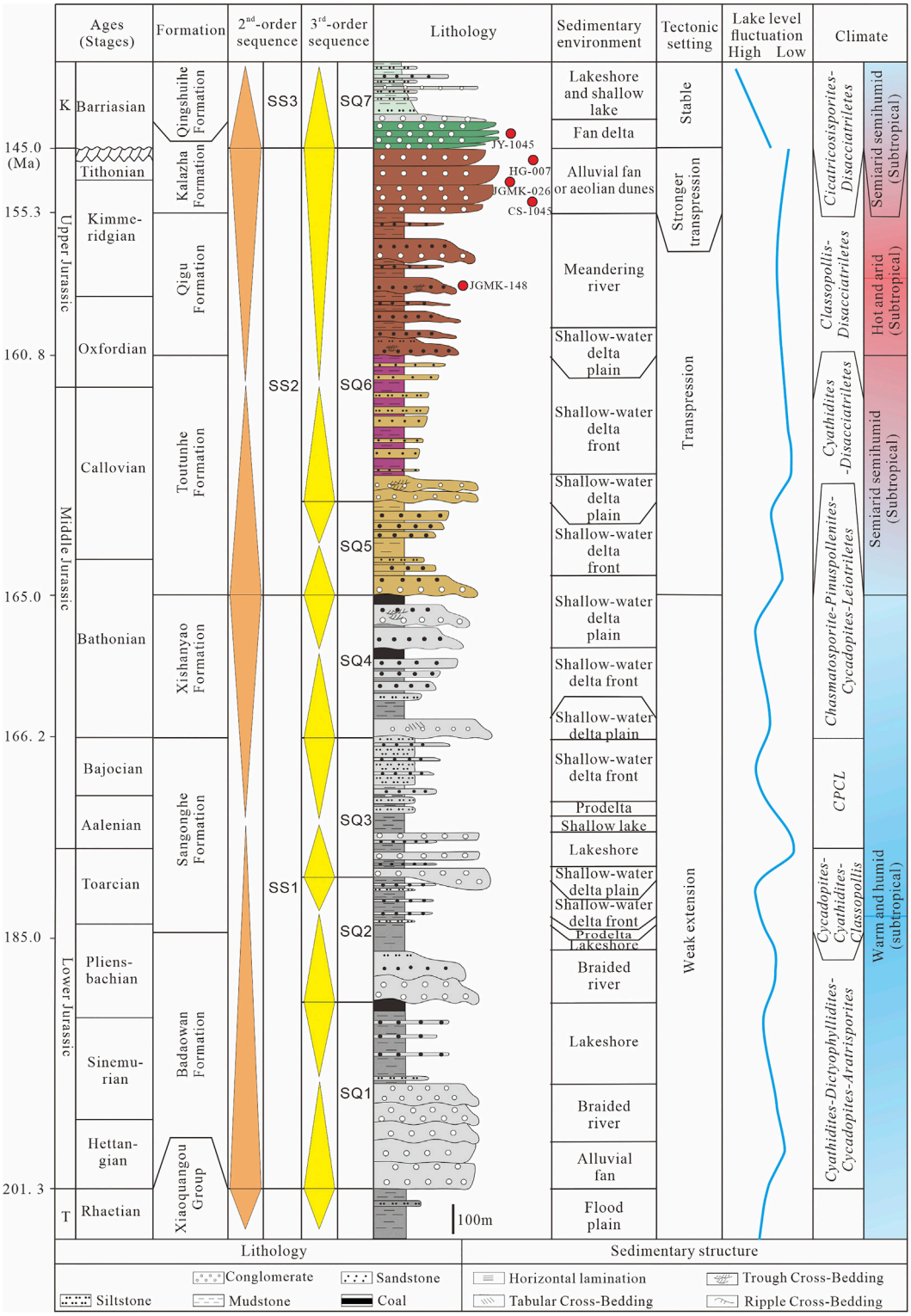

FIGURE 2 | Comprehensive stratigraphic column of the Southern Junggar Basin. T-Triassic; K-Cretaceous; CPCL-Chasmatosporite-Pinuspollenites-Cycadopites-Leiotriletes. Ages are from Deng et al. (2015) and Huang (2019). The spore-pollen assemblage and climate data are from Deng et al. (2015) and Tian (2017).

associated with the aridification, while some researchers assumed that the conglomerates were triggered by the far-field effect of collisions along the Asian margins (Hendrix et al., 1992; Fang et al., 2006b; De Grave et al., 2007; Fang et al., 2016).

To reconstruct the sedimentary and source-to-sink evolution in the SJB in the Late Mesozoic, we employed sedimentary analysis, paleocurrent, heavy mineral, and conglomerate component analysis combined with U-Pb age data of detrital zircons. This study provides insights into how tectonic and climatic evolution influence the source-to-sink system of intracontinental basins.

GEOLOGICAL SETTING

The Junggar Basin is believed to be a Permian rift basin (Fang et al., 2006a) and a Mesozoic to Paleocene intracontinental depression basin (Fang et al., 2004; Wu et al., 2004; Wang J. et al., 2018). The basin was in a post-orogenic weak extensional setting from the Early to Middle Jurassic, and the basin experienced transpression from the Middle Jurassic to the Late Jurassic, as evidenced by the rapid formation of the Chemo paleouplift (**Figures 1C**, **11C**), which is a transpressional structural belt (He et al., 2008; Ni et al., 2019). The Chemo paleouplift experienced initial development in the late part of the Early Jurassic, rapid growth and shaping from the Middle Jurassic (**Figures 1C**, **11C**), burial in the Cretaceous, and tilting and destruction in the Cenozoic (He et al., 2008).

The SJB is situated in the northern piedmont of the Tianshan and Bogda Orogenic Belts and can be divided into three present tectonic units, including the Sikeshu sag, Qigu fault belt, and Fukang fault belt (**Figure 1B**). The Jurassic strata in the SJB include the Badaowan, Sangonghe, Xishanyao, Toutunhe, Qigu, and Kalazha Formations (**Figure 2**). The Kalazha Formation features greenish-brown and red conglomerates and gray sandstones in different places in the SJB (Guan et al., 2020). The Cretaceous strata include the Lower Cretaceous Tugulu Group and Upper Cretaceous Donggou Formation, which unconformably contacted with the Upper Jurassic strata. The Tugulu Group includes Qingshuihe, Hutibi, Shengjinkou, and Lianmuqin Formations from bottom to top (**Figure 2**). The Donggou Formation is absent in the Sikeshu sag.

The potential provenances in the late Mesozoic include the North Tianshan, Central Tianshan, and Bogda Orogenic Belts, a northeastern branch of the Tianshan Orogenic Belt, evidenced by the collected paleocurrents (**Figures 1B,C**). The North Tianshan, Central Tianshan, and Bogda Orogenic Belts experienced subduction–accretion in the Paleozoic (Windley et al., 2007). The North Tianshan Orogenic Belt is mainly composed of arc-related igneous and volcaniclastic rocks of Devonian to Carboniferous age (Han et al., 2011; Xiao et al., 2013). Ordovician–Silurian tuffaceous siliciclastic rocks, limestones, and Permian volcanic and terrestrial clastic rocks are also distributed in the North Tianshan Orogenic Belt. The Bogda Orogenic Belt comprises a bimodal volcanic-sedimentary rock series of Carboniferous-Early Permian age and upper Paleozoic-Cenozoic sedimentary rocks in the northern and southern margins of the foothills (Wang Y. et al., 2018).

Different from the North Tianshan and Bogda Orogenic Belt, the Central Tianshan Orogenic Belt comprises Precambrian basements with high-grade metamorphic suites. In addition, the Central Tianshan Orogenic Belt consists of early Paleozoic subduction-related arc-type igneous rocks, Permian–late Paleozoic post-collisional granitoids (Han et al., 2011), Cambrian–Carboniferous greenschists, slates, limestone, and volcanic-siliciclastic rocks (Gao et al., 1998).

METHODS

Sedimentary outcrops of the Late Jurassic–Lower Cretaceous successions are well preserved and exposed in the southern Junggar Basin. Thirteen sedimentary sections were surveyed, including Sikeshu River, Manasi, Qingshuihe River, Taxihe River, Queergou, Hutubi River, Jiangong mine, Dongwozi, Toutunhe River, Wangjiagou, Baiyanggou, Shuimohe section, Dahongshan sections (**Figure 1C**).

These sections all include Qigu and Kalazha Formations, and Tugulu Group, the sedimentary successions of which were measured (**Figure 8**). The sedimentary structures were described and the sedimentary environments were interpreted. The sedimentary environments of these sections and well CS1 and JY2 (**Figure 1C**) were compared (**Figure 8**).

Heavy Mineral Composition

A total of 597 heavy mineral data in 32 wells (**Figure 1C**) and 7 sedimentary sections (**Figure 1C**) were used for provenance analysis, among which 23 heavy mineral data were conducted in the Langfang Yuneng Rock and Mineral Processing Co., Ltd. in Langfang, Hebei Province, and the other heavy mineral data were collected from Zhou et al. (2019). The detailed heavy mineral analysis process followed the methods described by Mange and Maurer (2012). Authigenic minerals were excluded from the analysis.

A matrix heatmap was used to represent individual values with different colors in the heavy mineral analysis (Zhu et al., 2017; Zhou et al., 2019). The heatmaps were generated by HemI version 1.0.3.3 software. The blue to red scale in the heatmaps represents low to high percentages of heavy minerals (Deng et al., 2014). Each column presents all the data for one specific heavy mineral from all the samples, and each row shows all the heavy mineral compositions of one specific sample. Different heavy mineral assemblages were generated by hierarchical cluster analysis using the average-linkage clustering algorithm. One pie chart on the heavy mineral assemblage distribution map for one specific stratum represents different heavy mineral assemblages indicating different source areas.

Conglomerate Components

The conglomerate outcrop data include conglomerate components and grain sizes from six sections, including Sikeshu River, Manas, Taxi River, Quergou, Baiyanghe, and Dongwozi section (**Figure 1**). In each section, ca. 100 clasts were counted in an area of 1 m^2 to analyze the provenance. The lithology of the conglomerate grains was identified in the field (see **Supplementary Figure S4**) and checked under an optical microscope with thin sections.

Detrital Zircon Geochronology

The detrital zircon geochronology of five samples was conducted in this study, including JGMK-026 (Kalazha Formation), HG-007 (Kalazha Formation), JY-2718 (Qingshuihe Formation), CS-1045 (Kalazha Formation), and JGMK-148 (Qigu Formation). We also collected detrital zircon geochronological data of eight published samples to compare with the new data, including sample SKSH-012 (Qingshuihe Formation, SKSH-052 (Qigu Formation, XJ10-016 (Qingshuihe Formation, Yang et al., 2013; Guan et al., unpublished data[1]), Tou-08 (Qingshuihe Formation, Fang et al., 2015), Tou-07 (Kalazha Formation, Fang et al., 2016), XJ09-100 (Qigu Formation, Yang et al., 2013), Tou-06 (Qigu Formation, Fang et al., 2015), TS12-110 (Qigu Formation, Tang et al., 2014). Sample SKSH-012 and SKSH-052 are from the Sikeshu River section (**Figure 1C**); sample JGMK-026 and JGMK-148 is from the Jiangong mine section (**Figure 1C**); the sample XJ10-016, XJ09-100, and HG-07 are from the Manas section (**Figure 1C**); sample Tou-08, Tou-07, Tou-06 are from the Toutunhe section (**Figure 1C**); sample TS12-110 is from Baiyanghe section (**Figure 1D**); sample CS-1045 is from well CS1 (**Figure 1D**); sample JY-2718 is from well JY2 (**Figure 1D**).

After separation by standard heavy liquid and magnetic techniques, 250 detrital zircon grains were randomly purified under a binocular microscope for each sample. The grains from samples JGMK-026 and HG-007 underwent cathodoluminescence (CL) imaging with a Quanta 200 FEG scanning electron microscope and U–Pb isotope analyses with LA–ICP–MS (Agilent 7500c ICP–MS coupled with a 193-nm ArFExcimer laser) at the Key Laboratory of Orogen and Crust Evolution, Peking University; the grains from samples JY-2718, CS-1045, and JGMK-148 underwent CL imaging and U–Pb isotope analyses using LA–ICP–MS (Agilent 7900 ICP–MS coupled with ATL (ATLEX 300) excimer laser and a two-volume S155 ablation cell) at Beijing GeoAnalysis Co., LTD. The analysis procedures proposed by Yuan et al. (2004) were followed. Isotopic ratios and elemental concentrations of zircon grains were calculated using the GLITTER 4.0 program (Jackson et al., 2004). Common lead was corrected using the method of Andersen (2002). The age calculations were performed using ISOPLOT 3 (Ludwig, 2003). The $^{207}Pb/^{206}Pb$ age was utilized when the age was >1,000 Ma, and the $^{206}Pb/^{238}U$ age was utilized when the age was <1,000 Ma. Only ages with concordance degrees >90% were analyzed (**Supplementary Figures S2, S3**).

RESULTS

Petrography, sedimentary analysis, heavy mineral assemblages, conglomerate components, and detrital zircon geochronology were conducted for source-to-sink analysis in the SJB.

[1]Guan, X., Wu, C., Zhang, X., Zhou, T., Tang, X., Xie, L., et al. (2021). Geochemistry of Detrital Ilmenite, Cr-Spinel, and Zircon U–Pb Geochronology: a Source-To-Sink Analysis of a Mesozoic Terrestrial Rift basin (Sikeshu Sag, Junggar Basin, NWChina). Int. Geology. Rev. Under review.

Petrological Characteristics

Based on field investigations, eleven lithofacies were delineated in the SJB (**Table 1**; **Figure 3**), including fine, sandstone, and conglomerate lithofacies. Fine lithofacies consist of Fsm and Fl lithofacies (**Table 1**). The lithologies include centimeter-to decimeter-thick fine sandstones, siltstones, siltstones, or mudstones (**Figures 3A,B**); the sandstone lithofacies include Sr, Sc, Sm, Sh, Sp, St, and SGF lithofacies (**Table 1**). These sandstone lithofacies have different sedimentary structures and were formed *via* different depositional processes (**Table 1**; **Figures 3C–F**). The conglomerate lithofacies is composed of Gmm and Gcm lithofacies (**Table 1**). The Gmm lithofacies is composed of granule to pebble beds that are tens of meters thick and matrix-supported (**Figure 3G**), while the Gcm lithofacies comprises decimeter-to meter-thick granule beds and is clast-supported (**Figure 3H**). The conglomerate components of Gmm lithofacies include both well-rounded gravels and poor-rounded gravels. The.

Seismite structures were observed in layered sheet-flow deposits with Gmm and Sm lithofacies, occurring in the Kalazha Formation in the Manas, Taxi River, Quergou, Jiangong mine, Baiyanghe, and Shuimohe section (**Figures 4A,B, D–H**, and the Qigu Formation in the Manas section (**Figure 4C**). Some sandstone veins are distorted and cut into several pieces (**Figures 4A–D**). Water escape structures are also present (**Figures 4E–H**). Tube-like sandstone veins connect to different sandstone layers (**Figures 4G,H**). The seismite structure extends laterally for hundreds of meters. Sandstone or gravelly sandstone veins penetrate the underlying layers by 10 cm to several meters (**Figures 4A–F**). Seismites appear frequently in the middle part of the Kalazha Formation and constitute tens of high-frequency cycles (**Figure 4A**).

Facies Association and Sedimentary Interpretation

Eleven lithofacies have been distinguished and grouped into seven facies associations based on field investigations. Sedimentary environments have been interpreted respectively, including alluvial fan, fan delta, aeolian dune, meandering river, alluvial plain, lakeshore, and shallow lake (**Table 2**).

Facies Association 1 and 2: Alluvial Fan and Fan Delta

Facies associations 1 and 2 dominate in the Kalazha Formation from the latest Jurassic to the Early Cretaceous in the SJB and are composed of Gmm, Gcm, Sm, Sp, and St lithofacies (**Table 2**). Tens of meters-thick conglomerate lithofacies with meter-thick Sm lithofacies were observed in the SJB. In the Qingshuihe section, Taxihe River section, Quergou section, Dongwozi section, Baiyanghe section, and Shuimohe section, the red facies association 1 underlies the brownish-green facies association 2 (**Figures 5D,E**). These two facies associations are distinctive in color (**Figures 5D,E**) because the conglomerate lithofacies in the facies association 1 contains a large amount of red matrix, while the conglomerate lithofacies in the facies association 2 lacks a red matrix and includes more greenish mudstones or siltstones (**Figure 3G**). The conglomerate

TABLE 1 | Lithofacies of the Qigu, Kalazha, and Qingshuihe Formations in the late Mesozoic Southern Junggar Basin.

Lithofacies code	Lithology	Sedimentary structure	Depositional process
Fine lithofacies			
Fsm (**Figure 3A**)	Centimeter- to decimeter-thick fine sandstone, siltstone, or mudstone	Mudcracks, calcareous nodules, and bioturbations (Scoyenia) (**Figure 6F**)	Suspension fall-out with emersion events
Fl (**Figure 3B**)	Centimeter- to decimeter-thick fine sandstone, siltstone, or mudstone	Horizontally lamination. Thin layers of mudstones interbedded with siltstones, fine sandstones, and millimeter-thick gypsums	Slack water deposition alternating with overbanks or waning floods
Sandstone lithofacies			
Sr (**Figure 3D**)	Centimeter- to decimeter-thick fine to medium sandstone	Wave (**Figure 7G**) or current ripples and ripple lamination	Wave or current ripple migration
Sc (**Figure 3C**)	Centimeter- to decimeter-thick fine to medium sandstone	Convoluted structure	Hydroplastic or liquefied deformation
Sm (**Figure 3A**)	Meter-thick medium to coarse sandstones	No sedimentary structure	Rapidly deposited sediments
Sh	Centimeter- to decimeter-thick medium to coarse sandstones	Parallel bedding and current lineations	Tractive current with upper-flow regime
Sp	Decimeter-thick fine to coarse sandstone	Planer cross-bedding	2D bedform migration
St (**Figure 3E**)	Decimeter-thick medium to coarse sandstone	Trough cross-bedding (**Figure 6E**)	3D bedform (dunes) migration
SGF (**Figure 3F**)	Meter- or tens of meters-thick medium to coarse sandstone	Meter-thick high-angle trough cross-bedding	Wind ripple migration and grainfalls in flow separation zone
Conglomerate lithofacies			
Gmm (**Figure 3G**)	Tens of meters-thick granule to pebble beds	Matrix-supported	Rapidly deposited sediments
Gcm (**Figure 3H**)	Decimeter- to meter-thick granule beds	Clast-supported with occasional clast imbrications and horizontal alignments	Tractive current transported or reworked by waves

lithofacies in the facies association 1 comprises red, polymictic, poorly to medium sorted, and poorly to medium rounded conglomerates (**Figures 5A,B,J**, and **Supplementary Figures S4A, B, C, E**) and is strongly cemented by calcite (**Figure 5**I), while the conglomerate lithofacies in the facies association 2 mainly consists of greenish-brown, polymictic, medium-to well-sorted, and medium-to well-rounded conglomerates (**Figures 3G**, **5F**,K, and **Supplementary Figure S4F**) with some preserved primary intergranular pores (**Figure 5M** and **Figure 5O**). More Gcm lithofacies occur, and several thin red conglomerates can also be observed in the facies association 2. Both the facies associations 1 and 2 are composed of several cycles (**Figures 5A,B**).

Facies associations 1 and 2 are interpreted as the products of alluvial fan and fan delta environments, respectively (**Table 2**). The facies association 1 has coarsening-upward successions, which are assumed to be progradational alluvial fan deposits, while the facies association 2 has fining-upward successions, which are believed to be retrogradational fan delta deposits. In the facies association 1, the Gmm lithofacies is flatly interlayered with Sm lithofacies and constitutes at least four short-term cycles in the Manasi section, which are interpreted as sheet flow deposits in the middle fan subfacies (**Figures 5A,B**). In the Sikeshu River section, the Kalazha Formation shows no layers and is poorly rounded and poorly sorted, which is suggestive of debris flows of the root fan subfacies (**Figure 5C**). In the facies association 2, meter-thick fining-upward sandstone and conglomerate successions with scour bases (**Figure 5K**) and trough cross-bedding are interpreted as distributary channels, and meter-thick coarsening upward sandstone and conglomerate successions are interpreted as mouth bars.

Facies Association 3: Aeolian Dune

The facies association 3 prevailed during the deposition of the Kalazha Formation in the latest Jurassic, and it is composed of the meters- or tens of meters-thick SGF lithofacies in the SJB (**Table 2**; **Figures 5G–I**). The SGF lithofacies consist of meter- and tens of meters-thick grey medium to coarse sandstones with high-angle trough cross-bedding (**Figure 3F**). The grains are well-rounded and clast-supported. A great number of primary intergranular pores are preserved in the SGF lithofacies (**Figure 5**N).

The facies association 3 is interpreted as eolian dune deposits in an erg environment (**Table 2**). The SGF lithofacies was the product of wind ripple migration and grainfalls in flow separation zones.

Facies Associations 4 and 5: Meandering River and Alluvial Plain

The facies association 4 is composed of Gcm, Sp, St, Sr, and Fsm lithofacies, and the facies association 5 consists of Sr, Fsm, and Fl lithofacies (**Table 2**). These facies associations are widespread in the Late Jurassic Qigu Formation. Facies associations 5 are also identified in the Kalazha Formation, with dominant mudstone lithofacies and thin layers of lens-shaped Sr lithofacies. A typical facies association 4 occurs in the Manasi and Jiangong mine sections. The upper part of the Qigu Formation mainly contains isolated lens-shaped sandbodies with thicknesses of 3–5 m (**Figure 6A**), while the lower part of the Qigu Formation

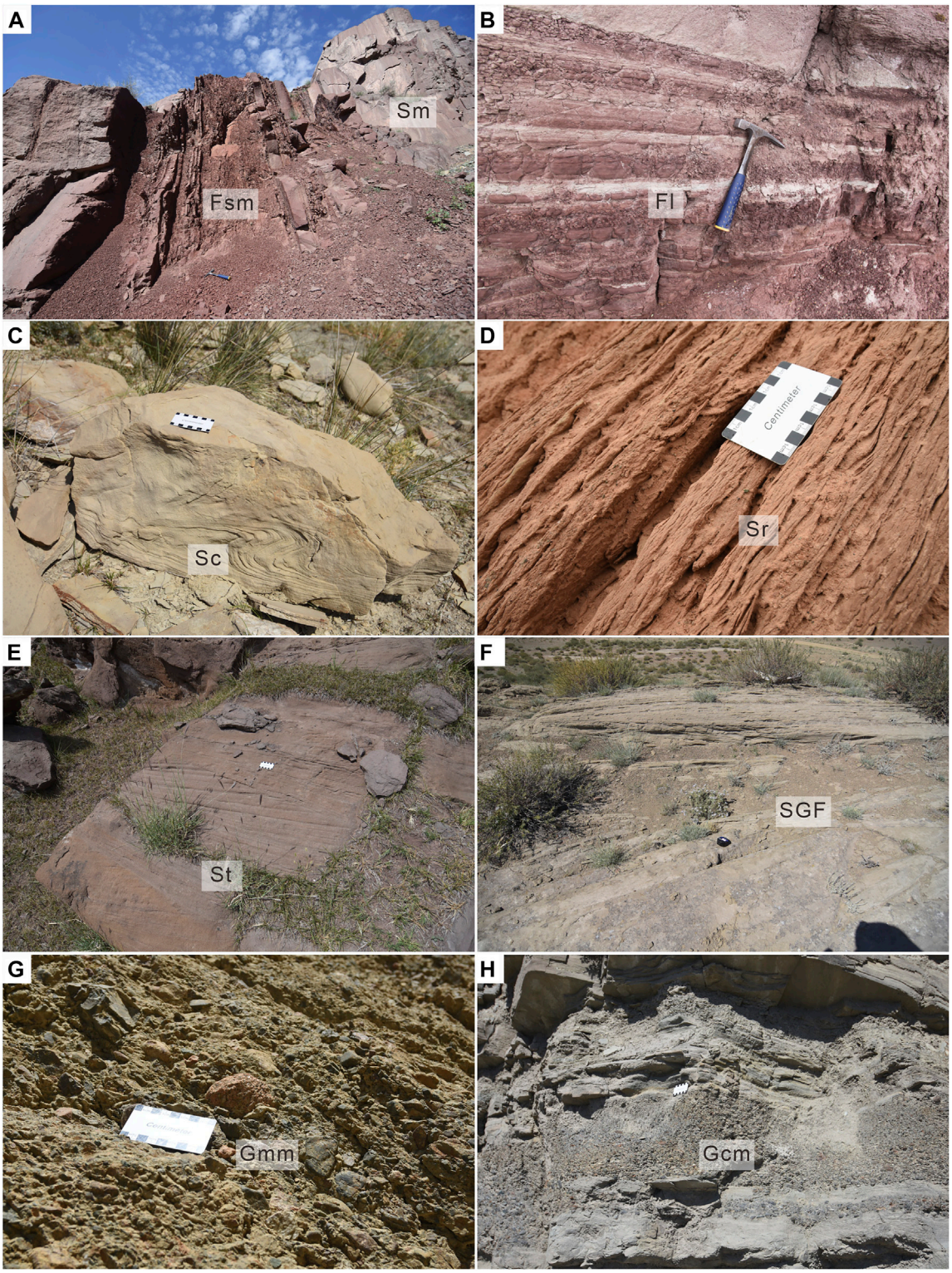

FIGURE 3 | Typical lithofacies in the late Mesozoic Southern Junggar Basin. **(A)** Fsm and Sm, Kalazha Formation, Wangjiagou section; **(B)** Fl, Qigu Formation, Jiangong mine section; **(C)** Quergou section; **(D)** Sikeshu River section; **(E)** St, Qigu Formation, Quergou section; **(F)** SGF, Kalazha Formation, Wangjiagou Formation; **(G)** Gmm, Kalazha Formation, Jiangong mine section; **(H)** Gcm, Qinghsuihe Formation, Jiangong mine section. The definition of lithofacies see **Table 1**.

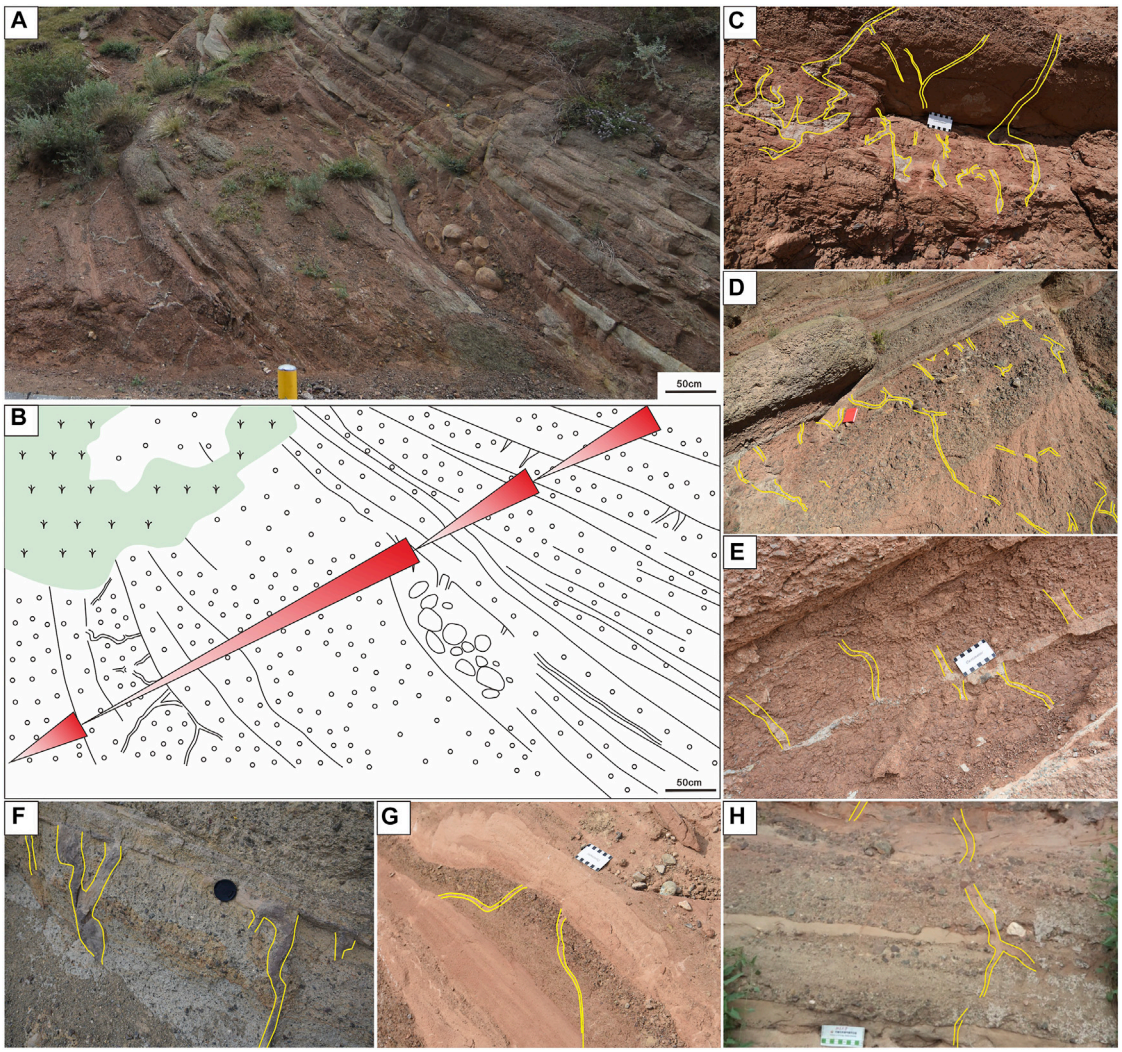

FIGURE 4 | Sedimentary characteristics of the seismites in the late Mesozoic Southern Junggar Basin **(A, B)** Quergou section, Kalazha Formation; **(C)** Manasi section, Qigu Formation (Guan et al., 2020). The ruler for scale; **(D)** Quergou section (Guan et al., 2020), Kalazha Formation. The notebook (17.5 cm) for scale; **(E)** Taxihe River section (Guan et al., 2020). The ruler for scale; **(F)** Jiangong mine section (Guan et al., 2020), Kalazha Formation. The lens cap (7.2 cm) for scale; **(G)** Baiyanghe section, Kalazha Formation. The ruler for scale; **(H)** Jiangong mine section (Guan et al., 2020), Kalazha Formation. The ruler for scale.

mainly contains bridging tabular or ribbon-like amalgamated bodies with thicknesses of 3–10 m (**Figure 6B**). Inclined thin mudstone layers in the sandbody are also observed. In a single sandbody, a small amount of lag gravel (Gcm lithofacies) or red mud clasts are developed at the bottom. The lower part of the sandbody is composed of Sp and St lithofacies (**Figure 6E**), and the upper part constitutes Sr and Fsm lithofacies with 1–2 m thick sandbodies (**Figure 6B**) and trace fossils, like Scoyenia ichnofacies (**Figure 6F**), were found.

The facies association 4 is interpreted as a meandering river environment (**Figures 6A,B**), and the facies association 5 is interpreted as an alluvial plain and overbank environment (**Figure 6C** and **Table 2**). The sandbodies in the facies association 4 are composed of channel and lateral accretion deposits (**Figure 6B**) in the lower part and overbank deposits (**Figure 6C**) in the upper part.

Facies Associations 6 and 7: Lakeshore and Shallow Lake

The facies associations 6 and 7 both dominate in the Early Cretaceous Qingshuihe Formation. The facies association 6 is composed of Gcm, Sr, and Fsm lithofacies, and facies association 7 is composed of Sr, Fsm, and Fl lithofacies in the SJB (**Table 2**). The facies association 6 overlies the facies association 2 (**Figure 7A**). In the facies association 6, meter-thick Gcm lithofacies and decimeter-to meter-thick Sr lithofacies are interlayered with thin layers of Fsm lithofacies. The Gcm lithofacies in the facies association 6 is gray-colored, well-sorted, and well-rounded (**Figure 7D** and **Supplementary Figure S4D**). The sheet-like sandbodies in these two facies associations extend for kilometers. Ripples (**Figure 7G**), ripple cross-bedding, mud cracks, and trace fossils, such as Scoyenia ichnofacies, are found. The grains

TABLE 2 | Facies associations and depositional environments in the late Mesozoic Southern Junggar Basin.

Facies association	Formation	Sedimentary architecture	Depositional environment
Facies association 1—Gmm, Gcm, Sm, Sp, St	Kalazha Formation	Tens of meters-thick Gmm facies, with meter-thick Sm facies, and some Gcm, Sp, and St facies (**Figures 5A,B, C, J**). Seismite structures can be observed (**Figures 4A,B,D,E,G**)	Alluvial fan deposits mainly composed of debris and sheet flows
Facies association 2—Gmm, Gcm, Sm, Sp, St	Kalazha Formation	Tens of meters-thick Gmm and Gcm facies, with some Sp and St facies in the lower succession (**Figures 5F**,K, **7A**,**B**). Seismite structures can be observed (**Figures 4F,H**)	Fan delta
Facies association 3—SGF	Kalazha Formation	Meter- or tens of meters-thick SGF facies (**Figures 5G,H**)	Eolian dunes in erg environment
Facies association 4—Gcm, Sp, St, Sr, Fsm	Qigu Formation	Meter-thick tabular or ribbon-like St facies with some Sp, St, Sr, and Fsm facies in the upper succession (**Figure 6 A, B**). Some Gcm facies are developed at the bottom of the sandbodies. Trough or tabular cross-beddings (**Figure 6E**), and scoyenia ichonfacies (**Figure 6F**) can be observed	Meandering river deposits with channels and lateral accretion architectural elements
Facies association 5—Sr, Fsm, Fl	Qigu Formation, Kalazha Formation	Meter-thick Fsm and Fl facies, with lens-shaped Sr facies (**Figure 6C**)	Alluvial plain and overbank deposits
Facies association 6—Gcm, Sr, Fsm	Qingshuihe Formation	Meter-thick Gcm facies and decimeter- to meter-thick Sr facies interlayered with thin layers of Fsm facies (**Figures 7A,B,D**). Waveripples (**Figure 7G**), ripple lamination, and ooids (**Figure 7F**) can be observed	Lakeshore environment
Facies association 7—Sr, Fsm, Fl	Qingshuihe Formation	Frequent alternation of Sr, Fsm, and Fl facies. In the Taxihe River section, millimeter-thick gypsum layers occur frequently (**Figure 7C**)	Shallow lake environment

are well-sorted, subrounded, and include ooids (**Figure 7F**). In the facies association 7, Sr, Fsm, and Fl lithofacies alternate frequently (**Figure 7C**). In the Taxihe River section, millimeter-thick gypsum layers occur frequently in the Qingshuihe Formation.

The facies association 6 is interpreted as a lakeshore environment, and the facies association 7 is interpreted as a shallow lake environment (**Table 2**). The facies associations 6 and 7 occur alternatively and frequently, which suggests frequent lake-level fluctuations.

Sedimentary Comparison

Meandering river environments prevailed during the deposition of the Qigu Formation in the SJB (**Figure 8**). The sedimentary environments in which the Kalazha Formation was deposited varied in the SJB. In the Sikeshu River and Manas sections, alluvial fan deposits developed in the Kalazha Formation (**Figure 8A**). The Manas section possesses the thickest facies association 1 (**Figure 8A**). In the Qingshuihe, Taxihe, Quergou, Hutubi, Jiangong mine, Dongwoz, Baiyanggou, and Shuimohe sections, and in well JY2 (**Figure 1C**), both alluvial fan and fan delta environments were identified in the Kalazha Formation (**Figure 8A**). The Jiangong Mine section exhibits the thickest DF facies association (**Figure 8A**).

In the Toutunhe, Wangjiazhuang, and Dahongshan sections, and well CS1, eolian dunes in an erg environment were identified in the Kalazha Formation (**Figure 8B**). A lacustrine environment prevailed during the deposition of the Qingshuihe Formation in the SJB (**Figure 8**). The lakeshore environment evolved upward into a shallow lake environment from the bottom.

Heavy Mineral Assemblages

The characteristics of parent rocks in potential provenances, including heavy mineral assemblages, are summarized in **Table 3**. The heavy mineral assemblages of sedimentary sections and wells are presented in pie charts in the sedimentary comparison profiles (**Figure 8**). In the Sikeshu River section, an assemblage of epidote + ilmenite in the Qigu Formation evolves into an assemblage of ilmenite + epidote + sphene + magnetite in the Kalazha Formation and epidote + magnetite + ilmenite in the Qingshuihe Formation (**Figure 8A**); in the Manas section, an assemblage of epidote + magnetite in the Qigu Formation changes into an assemblage of barite + magnetite + zircon in the Kalazha Formation, which changes into an assemblage of epidote + ilmenite + leucoxene (**Figure 8A**); in the Qingshuihe section, an assemblage of ilmenite + magnetite in the Qigu Formation evolves into an assemblage of spinel + ilmenite + garnet in the Qingshuihe Formation (**Figure 8A**); in the Jiangong mine section, the primary heavy mineral in the Qigu Formation is epidote, which evolves into an assemblage of ilmenite + leucoxene + garnet in the Kalazha Formation and leucoxene + garnet + apatite in the Qingshuihe Formation (**Figure 8A**); in the Toutunhe section, the heavy mineral assemblage is epidote + magnetite in the Qigu Formation, which changes into an assemblage of ilmenite + garnet in the Kalazha Formation (**Figure 8A**); in well CS1, an assemblage of ilmenite + magnetite in the Kalazha Formation evolves into an assemblage containing primary magnetite in the Qingshuihe Formation (**Figure 8B**); in the Shuimohe section, an assemblage of epidote + magnetite + ilmenite in the Qigu Formation changes into an assemblage of magnetite + zircon + epidote + garnet in the Kalazha Formation, which changes into an assemblage of epidote + magnetite + ilmenite (**Figure 8B**). The content of epidote increases from the bottom of the Kalazha Formation to the Qingshuihe Formation (**Figure 8B**); in well JY2, the heavy mineral assemblage is ilmenite + zircon + magnetite in the Qingshuihe Formation (**Figure 8B**).

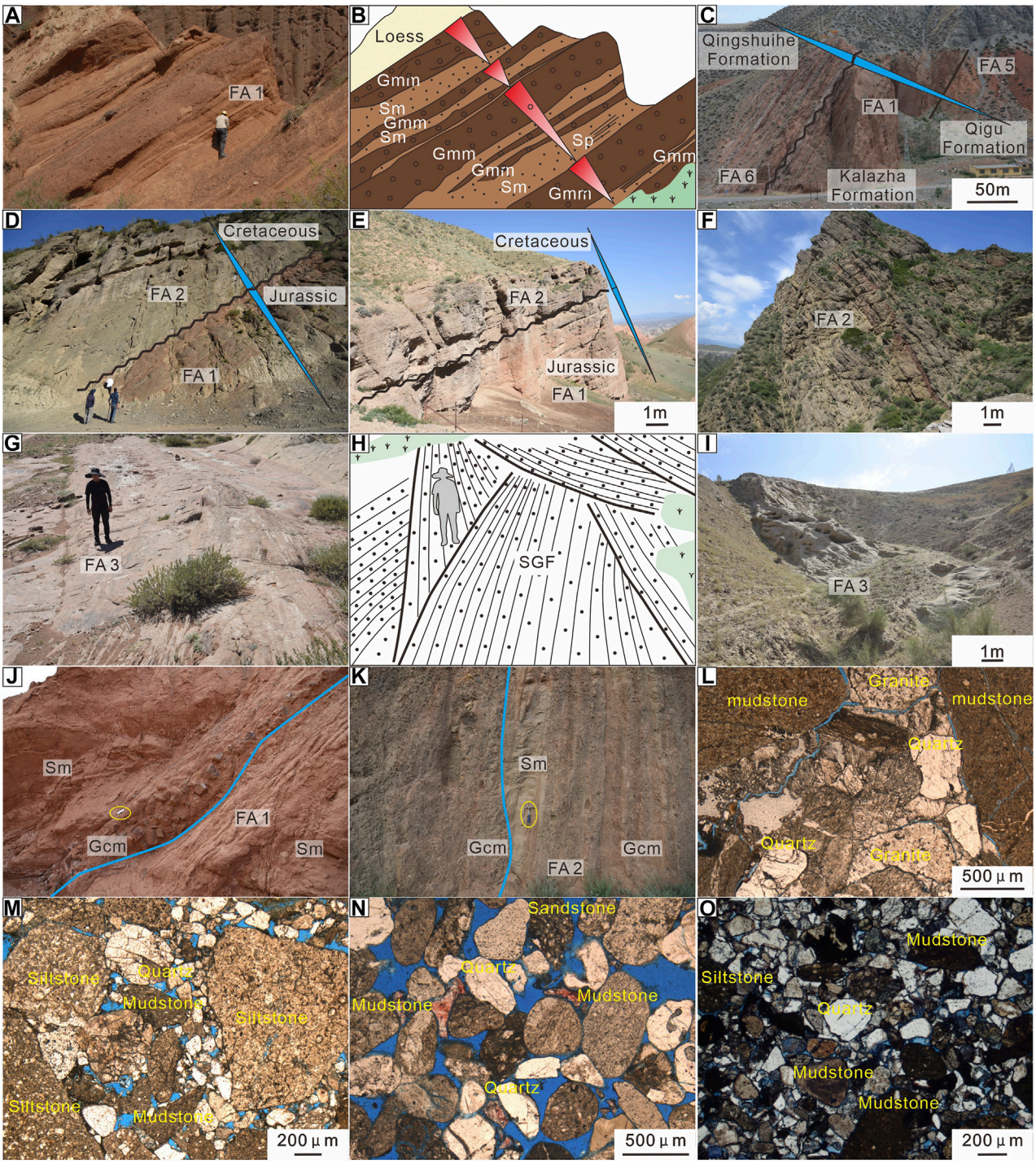

FIGURE 5 | Sedimentary characteristics of the Kalazha Formation in the northern piedmont of the Tianshan Orogenic Belt (a-f, l, m) and Bogda Orogenic Belt (g-k, n, o) in the Southern Junggar Basin **(A, B)** Manasi section (Guan et al., 2020). The man (170 cm) for scale; **(C)** Sikeshu River section; **(D)** Quergou section (Guan et al., 2021). The man (175 cm) for scale; **(E)** Dongwoz section; **(F)** Jiangong mine section **(G, H)** Wangjiazhuang section. The man (175 cm) for scale; **(I)** Dahongshan section **(J)** Shuimohe section. The ruler for scale **(K)** Baiyanghe section. The hammer (27.9 cm) for scale **(L)** casting thin section, plane-polarized light, Manasi section **(M)** casting thin section, plane-polarized light, Jiangong mine section **(N)** casting thin section with Alizarin red S, plane-polarized light, Toutunhe River section. The Alizarin red S stained the calcite red **(O)** casting thin section, plane-polarized light, Baiyanghe section. FA-facies association. The definition of facies associations see **Table 2**.

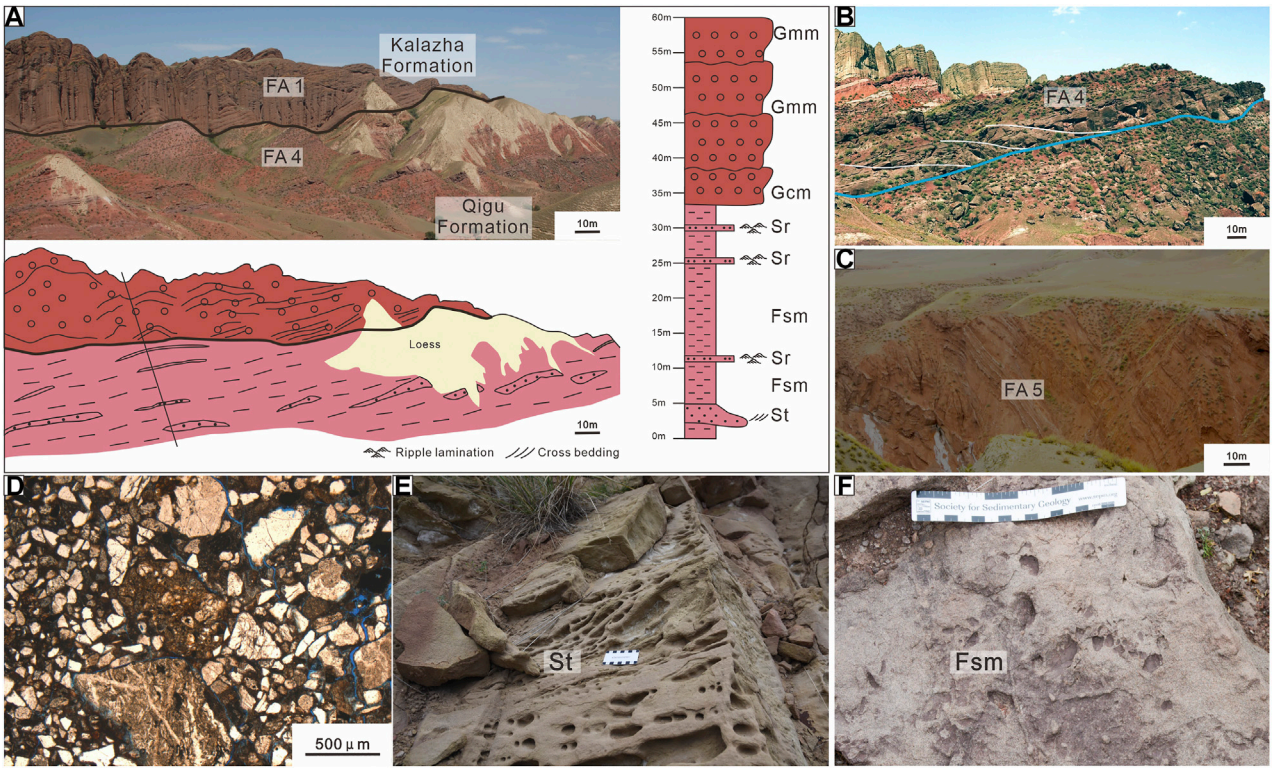

FIGURE 6 | Sedimentary characteristics of the Qigu Formation in the Southern Junggar Basin. **(A)** Manasi section; **(B)** Jiangong mine section (Guan et al., 2019); **(C)** Hutubi River section; **(D)** casting thin section, plane-polarized light, Manasi section; **(E)** cross-bedding, Taxihe River section. Mud clasts were weathered into cavities. The ruler for scale; **(F)** *Scoyenia* ichnofacies (Guan et al., 2019), Jiangong mine section. The ruler for scale. FA-facies association. The definition of facies associations see **Table 2**.

The heavy mineral assemblages in the Qigu and Qingshuihe Formations attained from the clustering analysis are shown in **Supplementary Table S1**. Five and four heavy mineral assemblages were identified in the Qigu and Qingshuihe Formations, respectively (**Figure 9**). According to these heavy mineral assemblages, three catchments were identified, which were located in the Sikeshu sag, Qigu fault belt, and Fukang fault belt (**Figures 1B**, **10**, **11**). The Sikeshu sag and Qigu fault belt are in the northern piedmont of the Tianshan Orogenic Belt and the Fukang fault belt is in the northern piedmont of the Bogda Orogenic Belt. The heavy mineral assemblages in catchments 1 to 3 in the Qigu Formation are magnetite + epidote + ilmenite, epidote + ilmenite + leucoxene, and epidote + leucoxene (**Figure 9A**); the heavy mineral assemblages in catchments 1 to 3 in the Qingshuihe Formation are epidote + ilmenite + garnet, ilmenite + garnet + epidote, and epidote + ilmenite + zircon + leucoxene + garnet (**Figure 9C**). In summary, ilmenite and epidote are common heavy minerals in the SJB (**Table 4**). The Qigu, Kalazha, and Qingshuihe Formations have abundant epidote, magnetite, and garnet, respectively (**Table 4**).

Conglomerate Components

The conglomerate components in the Kalazha and Qingshuihe Formations are shown in pie charts (**Figure 9B**) and **Table 4**. In catchment 1, the primary conglomerate component is mudstone in the Kalazha Formation; in catchment 2, the conglomerate components mainly include sandstone, mudstone, granite, tuff, and andesite in the Kalazha Formation; and in catchment 3, the conglomerate components are primarily composed of siltstone and andesite in the Kalazha Formation (**Figure 10B**). The primary conglomerate components in the Qingshuihe Formation evolved into siltstone and mudstone (**Figure 10B**).

Detrital Zircon Geochronology

The detrital zircon U–Pb ages of five samples (JGMK-148, JGMK-026, HG-007, CS-1045, and JY-2718) and eight collected samples in the late Mesozoic SJB are given in **Supplementary Material S2**. All the detrital zircons of the five samples are magmatic in origin because of their clear oscillatory zoning (**Supplementary Figure S1**) and high Th/U ratios (see **Supplementary Material S3**).

The reported crystallization ages of the intermediate-acidic igneous rocks of the North Tianshan, Central Tianshan, and Bogda Orogenic Belts are shown in histograms (**Figure 10**). All the age data are categorized into seven populations shown in pie charts (**Figure 10**): Precambrian (2,623–542 Ma), Cambrian–Devonian (541–359 Ma), Mississippian (359–318 Ma), Pennsylvanian (319–299 Ma), Permian (298–251 Ma), Triassic (250–200 Ma), and Jurassic (199–145.5 Ma). Samples 19-SKSH-052, XJ09-100, JGMK-148, HG-007, JY-2718, CS-1045, and

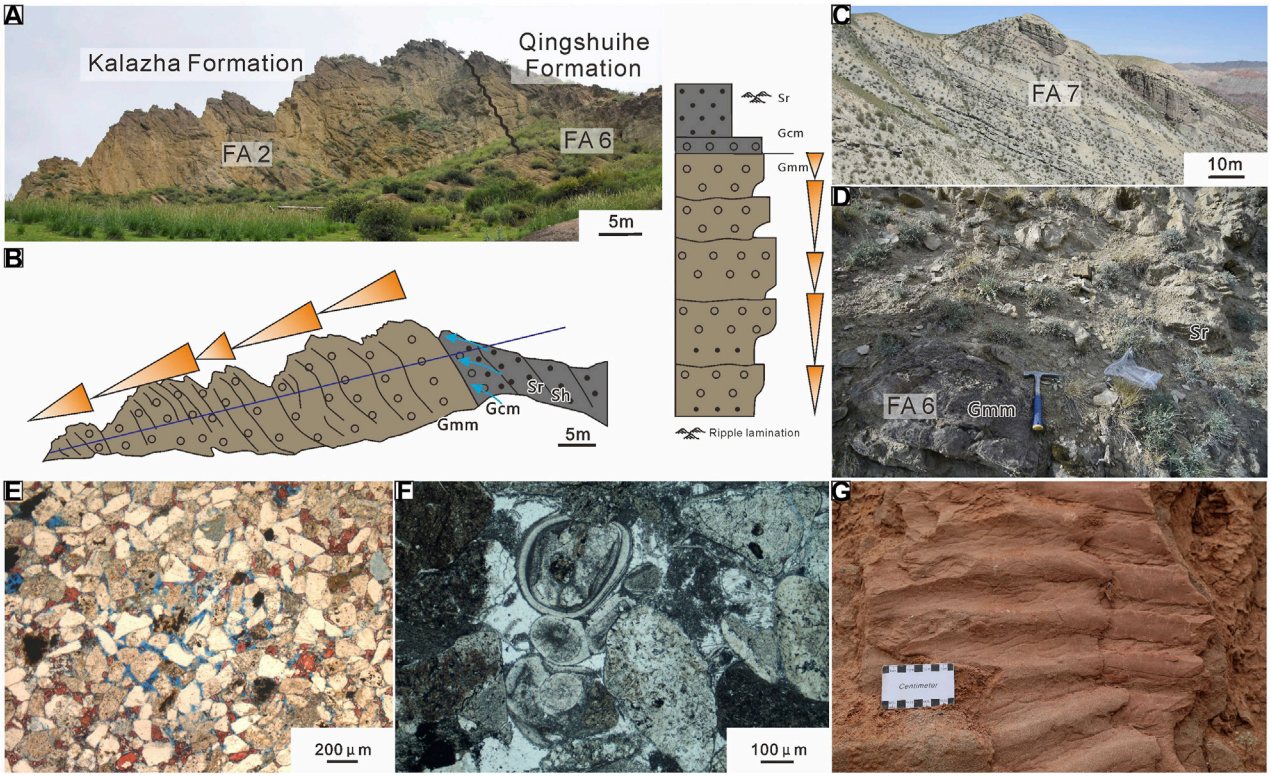

FIGURE 7 | Sedimentary characteristics of the Qingshuihe Formation in the Southern Junggar Basin **(A–D)** Jiangong mine section (Guan et al., 2020). The hammer (27.9 cm) for scale in d; **(E)** casting thin section with Alizarin red S, plane-polarized light, Manasi section. The Alizarin red S stained the calcite red; **(F)** thin section, plane-polarized light, Dongwoz section; **(G)** wave ripples, Sikeshu River section. The ruler for scale. FA-facies association. The definition of facies associations see **Table 2**.

TS12-110 have Jurassic age spectrum peaks of ca. 160 Ma (**Figure 10**); sample JGMK-026 has a Jurassic age spectrum peak of 156 Ma, and samples Tou-06 and Tou-07 have Jurassic age spectrum peaks of 154 Ma (**Figure 10**). Most of the thirteen samples have Precambrian zircons, except samples JGMK-148, JY-2718, and CS-1045 (**Figure 10**). Samples 19-SKSH-052, JGMK-148, and Tou-06 have similar age spectra and more Jurassic zircons than sample XJ09-100 (**Figure 10**).

Although sample JGMK-026 from the Kalazha Formation has more Precambrian ages, the age spectra of samples JGMK-026 and HG-007 from the Kalazha Formation are similar (**Figure 10**). Sample Tou-07 has more Permian and Triassic zircons than samples HG-007 and JGMK-026 from the Kalazha Formation (**Figure 10**).

The age spectra of the Qingshuihe sandstones in the catchment 3 (sample JY-2718) differs from the counterparts in the catchment 1 and 2 (sample SKSH-12, XJ10-016, and Tou-08), because it has an apparent Jurassic age spectrum peak (**Figure 10**). The age spectra of Qingshuihe sandstones in catchments 1 and 2 have strongly varied age distributions and have more Permian to Precambrian zircons (**Figure 10**). The Qingshuihe sandstone in the catchment 3 (sample JY-2718) has more Carboniferous zircons and fewer Jurassic zircons than the Qigu and Kalazha sandstones (samples TS12-110 and CS-1045) (**Figure 10**).

DISCUSSION

The evolution of the source-to-sink system of SJB is reconstructed based on a comprehensive provenance analysis. By analyzing the source-to-sink system evolution of the SJB, the climatic and tectonic evolution is implied.

Provenance Analysis

The paleocurrent data indicate that the main provenance was to the south of the SJB (**Figures 1C,D**). The potential provenances of catchments 1 and 2 in the northern piedmont of the Tianshan Orogenic Belt include the North Tianshan and Central Tianshan Orogenic Belt; the potential provenances of catchment 3 in the northern piedmont of the Tianshan Orogenic Belt include the Bogda, North Tianshan, and Central Tianshan Orogenic Belt.

In the SJB, the North Tianshan Orogenic Belt mainly provided sediments to catchments 1 and 2, and the Bogda Orogenic Belt primarily supplied sediments to catchment 3 in the Late Jurassic, which is suggested by proximal fluvial, alluvial, and fan delta environments (**Figure 8**). In addition, the detrital zircons also provide evidence. The detrital zircon age spectra of the samples in catchments 1 and 2 are compared with the reported crystallization ages of the intermediate-acidic igneous rocks of the North Tianshan and Central Tianshan Orogenic Belt (**Figure 10**). The distributional ranges of the Kalazha

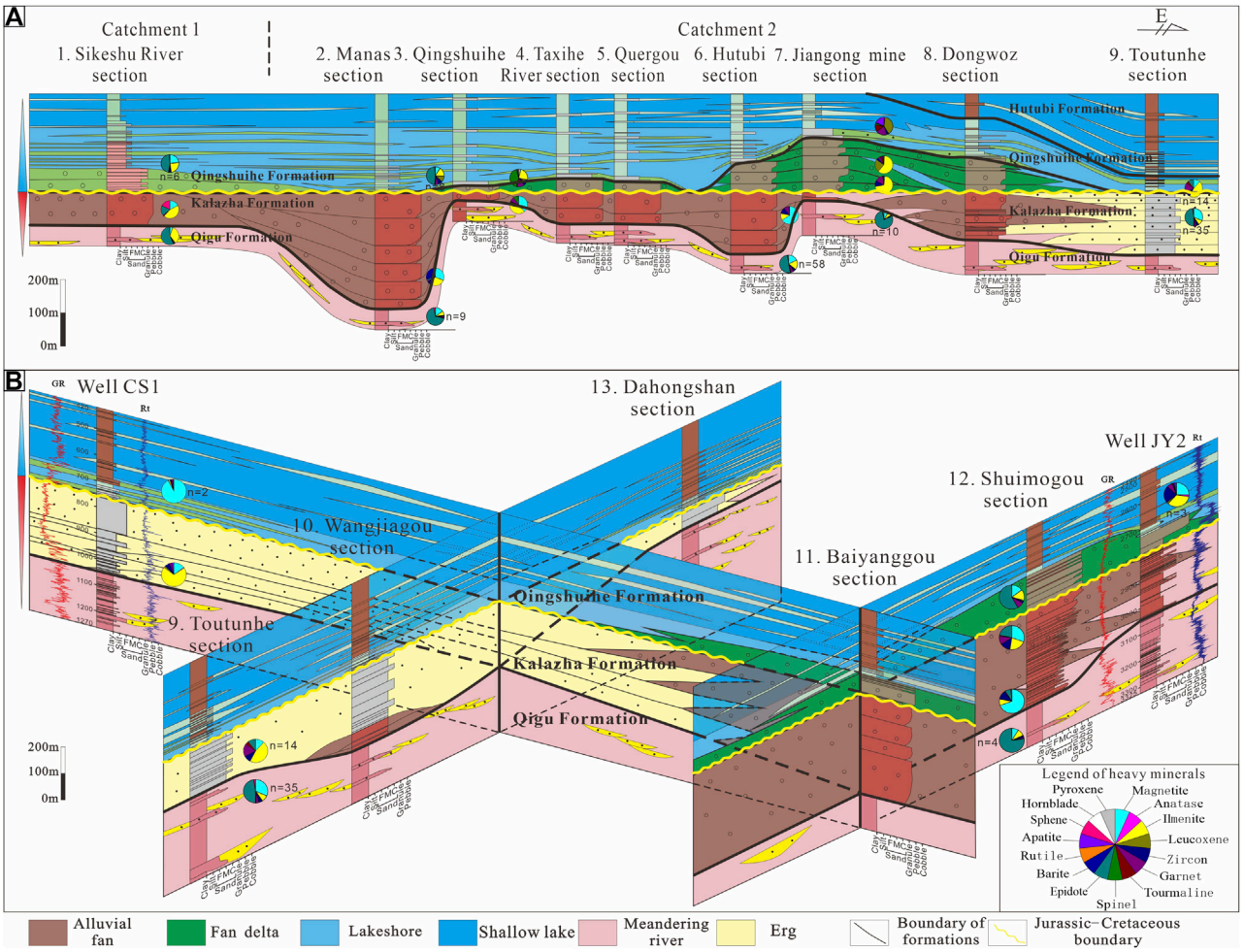

FIGURE 8 | Sedimentary comparison and heavy mineral assemblages in the northern piedmont of the Tianshan **(A)** and Bogda Orogenic Belts **(B)** in the late Mesozoic in the Southern Junggar Basin.

TABLE 3 | Characteristics of parent rocks of potential provenances.

Provenance	Age of parent rock/Ma	Lithology of parent rock	Heavy mineral assemblage
North Tianshan Mountains	266–386, 404–418, 434–466	Intermediate-acidic volcanic rocks, volcanoclastic rocks and tuffs, ophiolite rocks, siliciclastic rocks, carbonate rocks	Zircon + Tourmaline + Ilmenite + Magnetite + Barite + Apatite
Central Tianshan Mountains	221, 247–516, 541, 562, 730–742, 785, 806, 882–969, 1,014, 1,402–1,409, 1,433–1,438, 1,453–1,458, 1812, 2,466	Late Paleozoic type A granite, early Paleozoic volcanic rocks and granite, medium-high grade metamorphic rocks	Zircon + Tourmaline + Magnetite + Leucoxene + Garnet + Epidote + anatase + Sphene
Bogda Mountains	278–347, 362, 366	Granite, rhyolite, volcanoclastic rocks, intermediate-basic volcanic rocks, gabbro	Zircon + Ilmenite + Tourmaline + Magnetite + Apatite

Formation samples in catchments 1 and 2 have a high level of compliance with the North Tianshan Orogenic Belt (**Figure 10**).

With Precambrian ages and metamorphic rock sources (**Table 3** and **Figure 10**), the Central Tianshan Orogenic Belt constantly supplied sediments to the SJB in the late Mesozoic, which is evidenced by epidotes in most of the heavy mineral assemblages (**Table 4**; **Figures 9A,C–E**) and Precambrian ages of most of the samples (**Figure 10**). More medium-to high-grade metamorphic rocks were denudated in the Early Cretaceous, which is evidenced by the garnets in the heavy mineral assemblages in the Qingshuihe Formation (**Table 4** and **Figure 10**), because the Central Tianshan exhibits medium-to

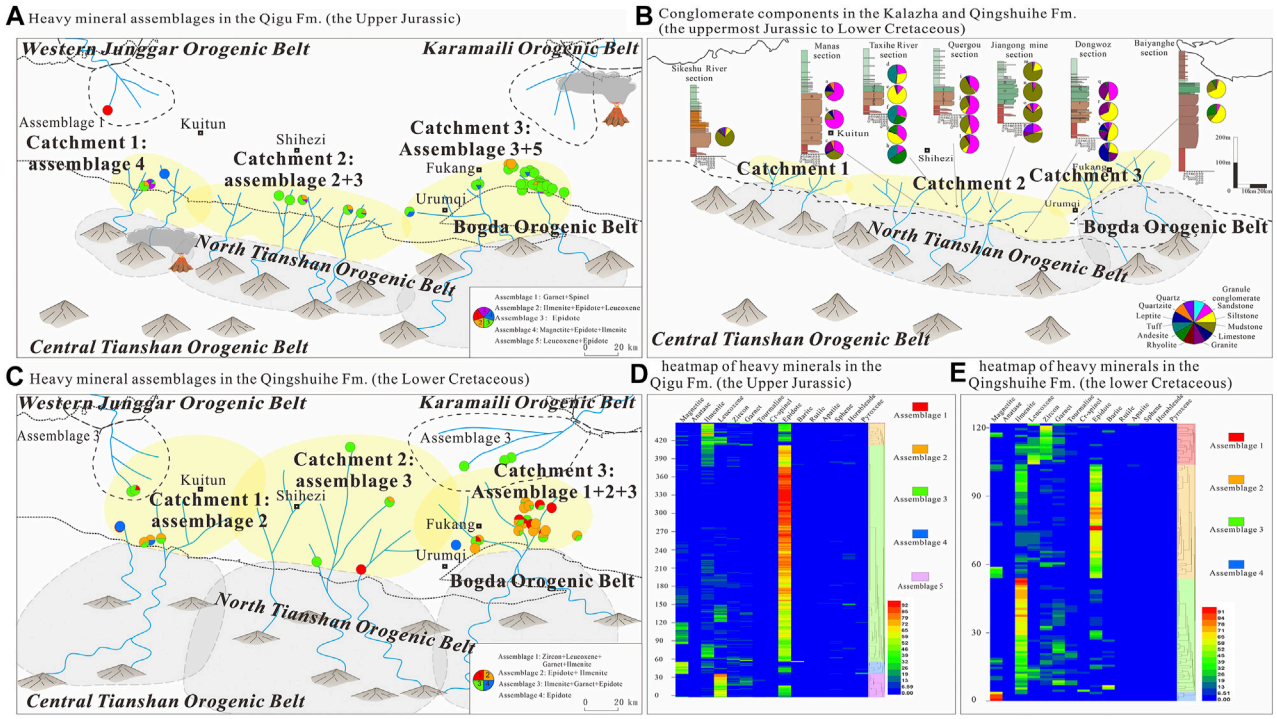

FIGURE 9 | Distribution of heavy mineral assemblages in the Southern Junggar Basin during the deposition of the Qigu **(A)** and Qingshuihe Formation **(B)** in the Late Jurassic and distribution of the conglomerate components during the deposition of the Kalazha and Qingshuihe Formation **(C)**. Heatmaps and clustering analysis were combined to analyze the heavy mineral assemblages in the Qigu Formation **(D)** and Qingshuihe Formation **(E)** using Heml version 1.0.3.3 software (Deng et al., 2014). The mineral percentages of each sample are shown in colors in the heatmaps (blue to red = low-to high-percentage contents). In the distribution map, pie charts represent the proportions of heavy mineral assemblages in wells and sedimentary sections. Fm., Formation.

high-grade metamorphic rocks that could have provided garnets. In addition, the distributional ranges of the Qingshuihe Formation samples in the catchments 1 and 2 have a higher level of compliance with the Central Tianshan Orogenic Belt (**Figure 10**). Therefore, it is inferred that source-to-sink systems expanded in the Early Cretaceous.

Denudation of the volcanoclastic or volcanic rocks of Late Jurassic ages was suggested by detrital zircon spectrum peaks of the Late Jurassic ages (154–162 Ma) in all samples (**Figure 10**). Although large-scale volcanic activities were not reported in the Junggar Basin and Tianshan area in the Mesozoic (Zhu et al., 2020), basalts, tuffs, tuffaceous sandstones, monzonitic granite, diorite, and trachyandesite of Jurassic ages provide direct evidence of Jurassic magmatism (Xu et al., 2008; Deng et al., 2015; Liu et al., 2018, 2019; Cao et al., 2020). The Late Jurassic age spectrum peaks (**Figure 10**) are absent in the age spectra of Lower and Middle Jurassic samples (Yang et al., 2013; Fang et al., 2015) and provide indirect evidence of Jurassic volcanism. Considering that Jurassic-age detrital zircons account for large percentages of the detrital zircons, igneous and volcaniclastic rocks were important source rocks in the Late Jurassic and may be extensively distributed around the Junggar Basin and Tianshan Orogenic Belt. Given that large-scale Late Jurassic altered zeolite and bentonite ores from volcanic ejection were found in the Wucaiwan area in the Eastern Junggar Basin (Cao et al., 2020) and that all the reported Meso-Cenozoic magmatic rocks are distributed near major strike-slip faults (Guo et al., 2010), the eruptive center was likely located in the Wucaiwan area in the Eastern Junggar Basin and along the North Tianshan Fault (Fang et al., 2015; Cao et al., 2020) (**Figure 9A**).

Sediment recycling happened in the basin margin in the late Mesozoic because red layers are observed in the brownish-green conglomerates in the Kalazha Formation, which are assumed that red Late Jurassic sediments were recycled in the earliest Cretaceous (**Figure 5F**). Besides, well-rounded gravels were found in the Kalazha Formation (**Figures 4A,B**; **Supplementary Figure S4C**).

In conclusion, the North Tianshan mainly provided sediments to catchments 1 and 2, and the Bogda Orogenic Belt primarily supplied sediments to catchment 3 in the Late Jurassic. The Central Tianshan Orogenic Belt constantly supplied sediments to the SJB in the late Mesozoic.

Sedimentary and Source-to-Sink System Evolution

From the Early to Middle Jurassic, with a warm and humid climate (Ashraf et al., 2010; Deng et al., 2015; Eberth et al., 2001; Hendrix et al., 1992; Li, et al., 2014), paludal environments dominated in the Early to Middle Jurassic, and coal seams were developed. Under a post-orogenic weak extensional tectonic setting, the Tianshan Orogenic Belt experienced

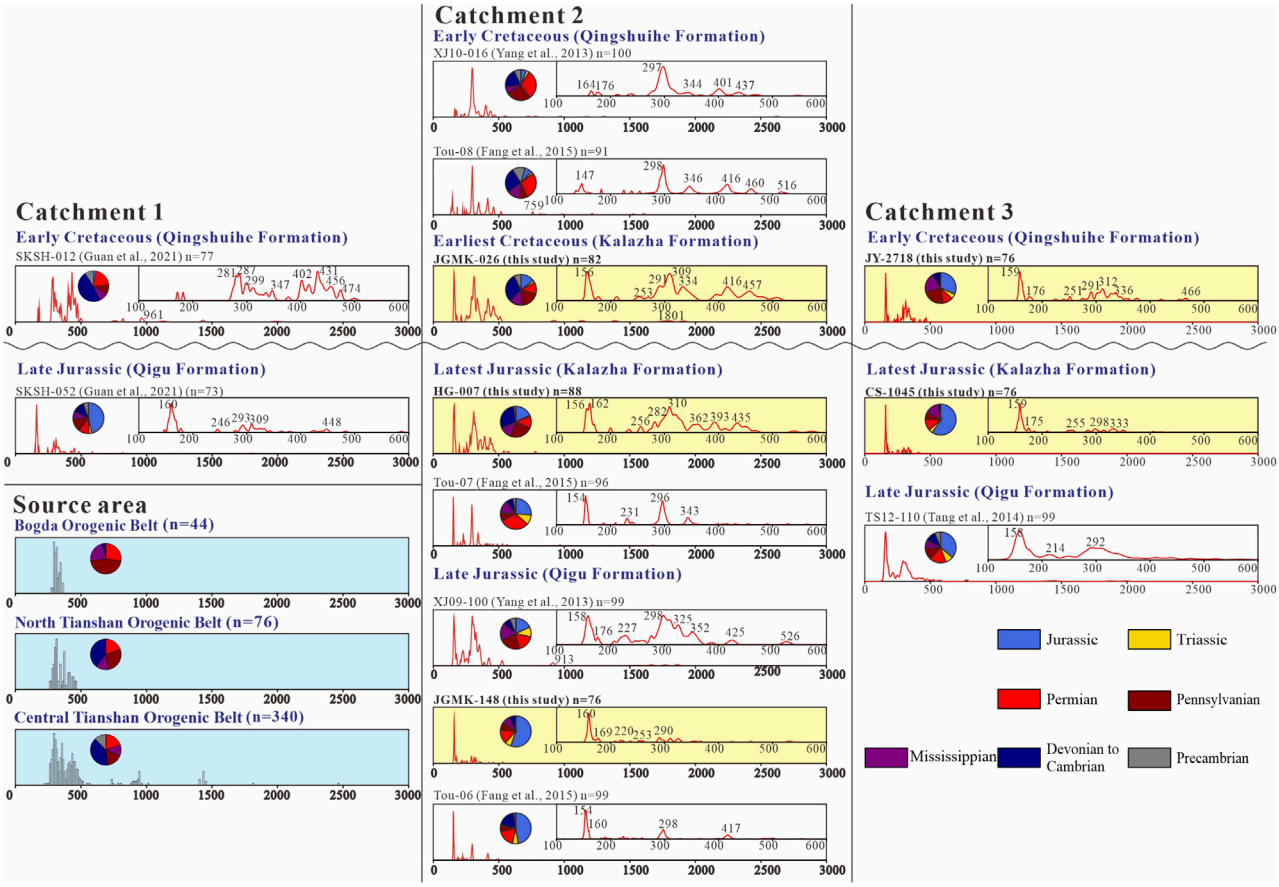

FIGURE 10 | Histogram of the crystallization ages from the Bogda, North Tianshan, and Central Tianshan Orogenic Belts (blue backgrounds) and the probability density plots of in the Southern Junggar Basin (catchments 1 and 2), including the 8 collected data (Yang, et al., 2013; Tang, et al., 2014; Fang et al., 2015). The samples with yellow backgrounds are from this study. The inset subgraphs display the probability density plots of the age distributions of zircons ranging from 600 to 100 Ma. The sample positions see *Detrital zircon geochronology* and **Figure 1C**. The samples above the wavy line are Cretaceous and the samples below the wavy line are Jurassic. Data for samples and source areas can be found in Supplementary Files S2 and S3, respectively.

TABLE 4 | Heavy mineral assemblages and conglomerate components of the late Mesozoic Southern Junggar Basin.

Strata	North piedmont of the tianshan mountains		North piedmont of the bogda mountains
	Catchment 1	Catchment 2	Catchment 3
Qigu Formation (Upper Jurassic)	Magnetite + Epidote + Ilmenite	Epidote + Ilmenite + Leucoxene	Epidote + Leucoxene
Kalazha Formation (latest Jurassic to earliest Cretaceous)	Ilmenite + Epidote + Magnetite + Sphene	Ilmenite + Magnetite + Leucoxene	Magnetite + Epidote + Zircon
	Mudstone	Sandstone + Mudstone + Granite + Tuff + Andesite	Siltstone + Andesite
Qingshuihe Formation (Lower Cretaceous)	Epidote + Ilmenite + Garnet	Ilmenite + Garnet + Epidote	Epidote + Ilmenite + Zircon + Leucoxene + Garnet
		Mudstone	Siltstone + Mudstone

peneplanation, sediments were transported from the Central Tianshan Orogenic Belt to the SJB (Yang et al., 2013; Fang et al., 2015, 2019). The western part of the Bogda Orogenic Belt exhibits slightly positive relief, which cannot block the sediments from the Tianshan Orogenic Belt (Fang et al., 2019). Sediments were transported from the North Tianshan to the Fukang fault belt (catchment 3), which is evidenced by northward paleocurrents and fluvio-lacustrine environments (Fang et al., 2019; Guan et al., 2021).

In the Late Jurassic, the tectonic setting evolved transpressional (He et al., 2018), and the North Tianshan and Bogda Orogenic Belts began to uplift, which is evidenced by a

cooling event shown in apatite fission data (Dumitru, et al., 2001; Guo et al., 2006; Shen et al., 2006, 2008; Tang et al., 2015). The tectonic activity was frequent, as evidenced by the frequent occurrence of the seismites in the Kalazha Formation (**Figure 4**). With the climate turning arid in the SJB (Fang et al., 2016; Jolivet et al., 2017), the coal-bearing strata changed into red beds in the late Middle Jurassic. The accommodation space decreased, and deltaic sedimentary environments gradually changed into fluvial environments, with sediments from the North Tianshan and Central Tianshan Orogenic Belt. The source areas include the Bogda and Tianshan Orogenic Belts (**Figure 9A**). In the latest Jurassic, the meandering river deposits turned into alluvial fan and eolian deposits during the deposition of the Kalazha Formation, with sediments mainly from the North Tianshan Orogenic Belt in catchments 1 and 2 and the Bogda Orogenic Belt in catchment 3. The source areas decreased and the source-to-sink systems shrank (**Figures 9B**, **11**). The Manas section was the depositional center of the alluvial fan deposits and the Wangjiagou section (**Figure 8A**) was the depositional center of the eolian deposits during the latest Jurassic (**Figure 8B**).

In the Early Cretaceous, the lake level rose. Fan deltas replaced the alluvial fans in the SJB during the deposition of the Kalazha Formation in the earliest Cretaceous. Sediments were mainly from the red alluvial fan deposits from the North Tianshan in catchments 1 and 2 and the Bogda Orogenic Belt in catchment 3. When the lake level rose to a high level and became relatively stable, accommodation space increased, and lacustrine environments prevailed. More sediments from the Central Tianshan were transported to the SJB, including sediments from medium-to high-grade metamorphic rocks. The source areas increased and source-to-sink systems expanded (**Figures 9C**, **11**). The depositional center changed from the Manas section to the Jiangong Mine section (**Figure 8A**).

A sequence boundary is identified between the facies associations 1 and 2 in the Kalazha Formation (**Figures 5D**,E, **8**), because the red facies associations 1 is assumed to be the highstand deposits of the Late Jurassic sequence (**Figure 2**) and the brownish-green facies association 2 is the lowstand deposit of the overlying sequence. According to *Facies association and sedimentary interpretation*, The facies association 1 is interpreted as alluvial fan, which is in conformable contact with the underlying Qigu Formation (**Figure 6A**), and facies association 2 is interpreted as fan delta. The reason why the facies association 1 was deposited before the facies association 2 is that red layers are observed in the brownish-green conglomerates in the Kalazha Formation, which are assumed that red Late Jurassic sediments were recycled in the facies association. Because of the lack of fossils and igneous rocks, the chronological attribution of the Kalazha Formation is hard to determine. The facies association 1 is assigned to the Kimmeridgian according to geochronological, cyclostratigraphic, and magnetostratigraphic studies by Deng et al. (2015). Because the lake transgressed extensively in the Early Cretaceous and the facies association 2 is interpreted as fan delta, the facies association 2 may be the product of lake transgression in the Early Cretaceous. Given that the facies association 2 is in conformable contact and has a gradational transition with the sandstone-dominated Qingshuihe Formation (**Figures 7A,B**; Eberth et al., 2001), the facies association 2 may be assigned to the Berriasian.

In summary, the sedimentary environments changed from paludal to fluvial and alluvial in the Late Jurassic, and evolved to fan deltaic and lacustrine in the Early Cretaceous. The source-to-sink system shrank in the Late Jurassic and expanded in the Early Cretaceous. Besides, a sequence boundary is identified between the facies associations 1 and 2 in the Kalazha Formation.

Implications for tectonics and Climate

The sedimentary and source-to-sink evolution of the intracontinental basin was controlled by tectonics and climate. The shrinkage of the catchment area and the lake in the Late Jurassic was caused by aridification in the Late Jurassic, which is suggested by red beds (**Figure 6**), eolian dunes (**Figures 5G–I**), gypsum, desiccation cracks, and the obvious increase in the spore genus *Classopollis* (Deng et al., 2015; Fang et al., 2016; Jolivet et al., 2017). The sediment flux was also reduced, as evidenced by the reduction in the thickness of the Qigu Formation. The source area also shrank in the Late Jurassic (**Figures 9A**, **11**), as evidenced by the heavy mineral assemblage and detrital zircon U-Pb data (**Figures 9A**, **10**), because the Tianshan and Bogda Orogenic Belts uplifted in the Late Jurassic, which is shown by apatite fission-track data (Dumitru, et al., 2001; Guo et al., 2006; Shen et al., 2006, 2008; Tang et al., 2015). Relatively high relief formed, which may have blocked part of the source area from the Central Tianshan Orogenic Belt. Additionally, the expansion of the catchment area (**Figure 9C**, **Figure 11**) in the Early Cretaceous was triggered by the semihumid climate, because the semihumid climate brought an increase in rainfall which led to an extensive lake transgression (**Figure 7**). The source area expanded in the Early Cretaceous, as suggested by the heavy mineral assemblage and detrital zircon U-Pb data (**Figures 9C**, **10**), which can be attributed to the reduction in the relief of the Tianshan and Bogda Orogenic Belts. More sediments from the Central Tianshan Orogenic Belt were transported to the SJB.

The conglomerates in the Kalazha Formation were attributed to both the tectonics and climate, because the arid environment can facilitate the destruction of the weathering profile and the exportation of coarse sediments during catastrophic rainfalls (Jolivet et al., 2017) and the uplift of the Tianshan and Bogda Orogenic Belts (Tang et al., 2014; Fang et al., 2019) can facilitate the denudation of the source area. During the deposition of conglomerates, tectonic activities were frequent which are recorded by several layers of seismites in the Kalazha Formations (**Figure 4**).

The coeval alluvial conglomerates with the Kalazha Formation were reported in the Tarim Basin (Jolivet et al., 2017), Turfan Basin (Yuan et al., 2002), Fergana Basin (Jolivet et al., 2017), Yarkand-Fergana Basin (Morin et al., 2020), Beishan (Zhao et al., 2003), and Yingen Basin (Wei et al., 2006) in Central Asia, which suggests the tectonic activity in the Late Mesozoic influenced vast area in Central Asia. The Kalazha Formation was related to the transpression in the Junggar Basin and the uplift of the Tianshan and Bogda Orogenic Belts in the Late Jurassic, which was caused

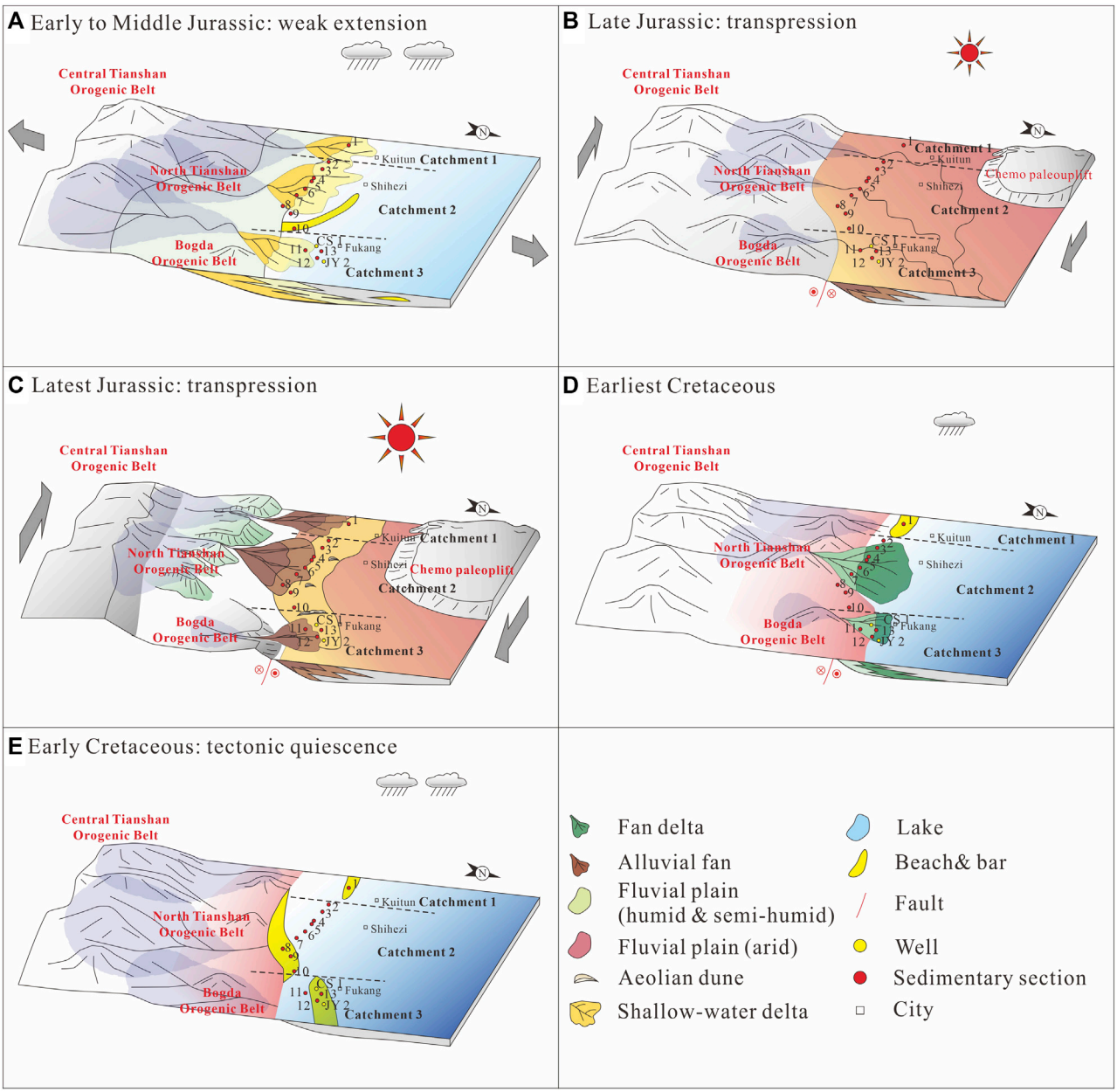

FIGURE 11 | Sedimentary and source-to-sink system evolution in the Southern Junggar Basin in the late Mesozoic. **(A)** Early to Middle Jurassic; **(B)** Late Jurassic; **(C)** latest Jurassic; **(D)** earliest Cretaceous; **(E)** Early Cretaceous. North Tianshan- North Tianshan; Central Tianshan- Central Tianshan. 1. Sikeshu River section; 2. Manasi section; 3. Qingshuihe River section; 4. Taxi River section; 5. Quergou section; 6. Hutubi section; 7. Jiangong mine section; 8. Dongwozi section; 9. Toutunhe section; 10. Wangjiagou section; 11. Baiyanggou section; 12. Shuimogou section; 13. Dahongshan section.

by dextral transpression of the boundary fractural zones in the Late Jurassic (He et al., 2008). This can be related to the far-field effect of the collision of the Lhasa Block along the southern margin of Asia (Hendrix et al., 1992; Li and Peng, 2013), the accretion of the Helmand Block to the southwestern Tianshan Orogenic Belt (Morin et al., 2018), or the rapid closure of the eastern part of the Mongol–Okhotsk Ocean (Yang et al., 2015a; Yang et al., 2015b). Because the collision of the Lhasa Block along the southern margin of Asia mainly occurred during the Early Cretaceous (Kapp et al., 2005; Yang et al., 2009), the collision of the Lhasa Block was unlikely to influence the Junggar Basin and the Mountains. Considering that the tectonic activity was stronger and earlier in the northern Junggar Basin (Cao et al., 2020) and that the Mongol–Okhotsk Ocean was located to the north of the Junggar Basin (**Figure 1A**), the far-field effect of the rapid closure of the eastern part of the Mongol–Okhotsk Ocean may be attributed to the uplift of the Tianshan and Bogda Orogenic Belts in the late Mesozoic.

The cause of aridification in the Late Jurassic has been debated. Hendrix (2000) assumed that the breakup of Pangea caused the cessation of the monsoon, which brought humid moisture to the Junggar Basin. Li et al. (2014) proposed that the collision of Lhasa and Qiangtang caused high relief and blocked humid moisture from the Tethys Sea. Yi et al. (2019) believed that a true polar wander with a southward displacement of ~25° displaced the Junggar Basin to a middle-latitude arid zone from a high-latitude humid-temperate zone and triggered aridification, as evidenced by paleomagnetic data. Given that the collision of the Lhasa and Qiangtang blocks mainly occurred during the Early Cretaceous (Kapp et al., 2005; Yang et al., 2009) and Pangea was still considerably intact in the Late Jurassic (Torsvik et al., 2012), the true polar wander hypothesis is more reasonable. The climatic change from arid to semihumid can also be explained by true polar wander because the Junggar Basin moved back to the semihumid zone, as suggested by paleomagnetic data (Yi et al., 2019).

In summary, the sedimentary and source-to-sink evolution of intracontinental basins is controlled by tectonics and climate (**Figure 11**). The succession in the Late Mesozoic was a response to the aridification in Central Asia and the uplift in the Bogda and Tianshan Orogenic Belt in the late Jurassic. The aridification may be triggered by the true polar wander in the Late Jurassic and the uplift of Bogda and the Tianshan Orogenic Belt may be the far-field effect of the rapid closure of the eastern part of the Mongol–Okhotsk Ocean.

CONCLUSION

Based on the sedimentary analysis, paleocurrent, heavy mineral, conglomerate component analysis, and detrital zircon U-Pb geochronology, we draw the following conclusions;

1. Seven facies associations, including alluvial fan, fan delta, aeolian dune, meandering river, alluvial plain, lakeshore, and shallow lake, have been identified and described in detail.
2. The sedimentary environments changed from paludal to fluvial and alluvial in the Late Jurassic, and evolved to fan deltaic and lacustrine in the Early Cretaceous.
3. Three source-to-sink systems are identified, according to different source-to-sink system features. The North Tianshan mainly provided sediments in the Late Jurassic in the northern piedmont of the Tianshan Orogenic Belt. The North Tianshan and Central Tianshan both supplied sediments in the Early Cretaceous. In the northern piedmont of the Bogda Orogenic Belt, the Bogda Orogenic Belt was constantly the primary provenance, and the Tianshan Orogenic Belt also provided sediments. Sediment recycling occurred in the basin margin in the Late Jurassic and more metamorphic rocks were denudated in the Early Cretaceous.
4. The source-to-sink systems shrank in the Late Jurassic and expanded in the Early Cretaceous. This source-to-sink evolution and Kalazha conglomerates with seismite structures responded to the aridification in the Late Jurassic, the uplift of the Bogda and Tianshan Orogenic Belts in the Late Jurassic, and the exhumation of the Bogda and Tianshan Orogenic Belts in the Early Cretaceous.

DATA AVAILABILITY STATEMENT

The original contributions presented in the study are included in the article/**Supplementary Material**, further inquiries can be directed to the corresponding authors.

AUTHOR CONTRIBUTIONS

Conceptualization: XG and CW; Data Acquisition and Methodology: XG and WZ; Analysis and Supervision: XZ and WJ.

FUNDING

This work was financially supported by the National Science and Technology Major Project of China (2017ZX05008-001).

ACKNOWLEDGMENTS

Many thanks to Dr. Yan Xu (Peking University) for constructive advice, as well as Dr. Yue Jiao, Dr. Jiaquan Zhou, Dr. Cong Lin, and Chufan Ren (Peking University) for their field assistance.

SUPPLEMENTARY MATERIAL

The Supplementary Material for this article can be found online at: https://www.frontiersin.org/articles/10.3389/feart.2021.785659/full#supplementary-material

REFERENCES

Andersen, T. (2002). Correction of Common lead in U-Pb Analyses that Do Not Report 204Pb. *Chem. Geol.* 192, 59–79. doi:10.1016/s0009-2541(02)00195-x

Ashraf, A. R., Sun, Y., Sun, G., Uhl, D., Mosbrugger, V., Li, J., et al. (2010). Triassic and Jurassic Palaeoclimate Development in the Junggar Basin, Xinjiang, Northwest China-a Review and Additional Lithological Data. *Palaeobio Palaeoenv* 90, 187–201. doi:10.1007/s12549-010-0034-0

Bally, A. W., and Snelson, S. (1980). "Realms of Subsidence," in *Facts and Principles of World Petroleum Occurrence*. Editor A. D. Miall (Canadian Society of Petroleum Geology), 6, 9–75.

Bhattacharya, J. P., Copeland, P., Lawton, T. F., and Holbrook, J. (2016). Estimation of Source Area, River Paleo-Discharge, Paleoslope, and Sediment Budgets of Linked Deep-Time Depositional Systems and Implications for Hydrocarbon Potential. *Earth-Sci. Rev.* 153, 77–110. doi:10.1016/j.earscirev.2015.10.013

Cao, Y., Chen, F., Paerhati, Z., Cao, X., and Meng, H. (2020). A Pilot Research on the Volcanic Event Deposits in the Junggar Basin in the Middle and Late Jurassic. *Xinjiang Geol.* 38, 32–34. [in Chinese with English abstract].

Carroll, A. R., Graham, S. A., and Smith, M. E. (2010). Walled Sedimentary Basins of China. *Basin Res.* 22, 17–32. doi:10.1111/j.1365-2117.2009.00458.x

De Grave, J., and Buslov, M. M. (2007). Distant Effects of India-Eurasia Convergence and Mesozoic Intracontinental Deformation in Central Asia: Constraints from Apatite Fission-Track Thermochronology. *J. Asian Earth Sci.* 29, 188–204.

Deng, W., Wang, Y., Liu, Z., Cheng, H., and Xue, Y. (2014). HemI: A Toolkit for Illustrating Heatmaps. *PloS one* 9, e111988.

Deng, S., Wang, S., Yang, Z., Lu, Y., Li, X., Hu, Q., et al. (2015). Comprehensive Study of the Middle-Upper Jurassic Strata in the Junggar Basin, Xinjiang. *Acta Geosci. Sin.* 36, 559–574. (in Chinese with English abstract).

Dumitru, T. A., Zhou, D., Chang, E. Z., Graham, S. A., Hendrix, M. S., Sobel, E. R., et al. (2001). "Uplift, Exhumation, and Deformation in the Chinese Tian Shan," in *Paleozoic and Mesozoic Tectonic Evolution of Central Asia: From Continental Assembly to Intracontinental Deformation*. Editors M. S. Hendrix and G. A. Davis (Geological Society of America), 194, 71–99. Memoir. doi:10.1130/0-8137-1194-0.71

Eberth, D. A., Brinkman, D. B., Chen, P.-J., Yuan, F.-T., Wu, S.-Z., Li, G., et al. (2001). Sequence Stratigraphy, Paleoclimate Patterns, and Vertebrate Fossil Preservation in Jurassic–Cretaceous Strata of the Junggar Basin, Xinjiang Autonomous Region, People's Republic of China. *Can. J. Earth Sci.* 38, 1627–1644. doi:10.1139/e01-067

Fang, S., Guo, Z., Zhang, Z., and Wu, C. (2004). Discussion on Mesozoic-Cenozoic Evolution of Tian Shan and its Adjacent Basins. *Acta Sci. Nat. Univ. Pekinensis* 40, 886–897. [in Chinese with English abstract]. doi:10.3321/j.issn:0479-8023.2004.06.006

Fang, S., Guo, Z., Jia, C., Zhang, Z., Wang, X., and Wang, M. (2006a). Meso-Cenozoic Heavy mineral Assemblages in the Southern Junggar Basin and its Implication for Basin-Orogen Pattern. *Chin. J. Geol.* 41, 648–662. [in Chinese with English abstract]. doi:10.3321/j.issn:0563-5020.2006.04.008

Fang, S., Jia, C., and Guo, Z. (2006b). New View on the Permian Evolution of the Junggar Basin and its Implications for Tectonic Evolution. *Earth Sci. Front.* 13, 108. [in Chinese with English abstract].

Fang, Y., Wu, C., Guo, Z., Hou, K., Dong, L., Wang, L., et al. (2015). Provenance of the Southern Junggar Basin in the Jurassic: Evidence from Detrital Zircon Geochronology and Depositional Environments. *Sediment. Geol.* 315, 47–63. doi:10.1016/j.sedgeo.2014.10.014

Fang, Y., Wu, C., Wang, Y., Hou, K., and Guo, Z. (2019). Topographic Evolution of the Tianshan Mountains and Their Relation to the Junggar and Turpan Basins, Central Asia, from the Permian to the Neogene. *Gondwana Res.* 75, 47–67. doi:10.1016/j.gr.2019.03.020

Fang, Y., Wu, C., Wang, Y., Wang, L., Guo, Z., and Hu, H. (2016). Stratigraphic and Sedimentary Characteristics of the Upper Jurassic-Lower Cretaceous strata in the Junggar Basin, Central Asia: Tectonic and Climate Implications. *J. Asian Earth Sci.* 129, 294–308.

Gao, J., Li, M., Xiao, X., Tang, Y., and He, G. (1998). Paleozoic Tectonic Evolution of the Tianshan Orogen, Northwestern China. *Tectonophysics* 287, 213–231. doi:10.1016/s0040-1951(97)00211-4

Graham, S. A., Hendrix, M. S., Wang, L. B., and Carroll, A. R. (1993). Collisional Successor Basins of Western China: Impact of Tectonic Inheritance on Sand Composition. *Geol. Soc. Am. Bull.* 105, 323–344. doi:10.1130/0016-7606(1993)105<0323:csbowc>2.3.co;2

Guan, X., Wu, C., Jian, W., Zhou, J., Jiao, Y., Zhou, R., et al. (2020). Sedimentary Sequence and Depositional Environment Evolution of Upper Jurassic-Lower Cretaceous Strata in the Southern Margin of Junggar Basin. *Xinjiang Pet. Geol.* 41, 67–79. [in Chinese with English abstract].

Guan, X., Wu, C., Zhou, T., Tang, X., Ma, J., and Fang, Y. (2021). Jurassic-Lower Cretaceous Sequence Stratigraphy and Allogenic Controls in Proximal Terrestrial Environments (Southern Junggar Basin, NW China). *Geol. J.* 56, 4038–4062. doi:10.1002/gj.4132

Guan, X., Wu, J., Wei, L., Zhao, J., Feng, G., and Li, Y. (2019). Meandering River Deposit and Sand Body Architecture in Qigu Formation of Jiangong Mine Section in the Southern Margin of Junggar Basin. *Xinjiang Petrol. Geol.* 40, 290–297. (in Chinese with English abstract)

Guo, Z., Zhang, Z., Wu, C., Fang, S., and Zhang, R. (2006). The Mesozoic and Cenozoic Exhumation History of Tianshan and Comparative Studies to the Junggar and Altai Mountains. *Acta Geol. Sin.* 80, 1–15. [in Chinese with English abstract].

Guo, Z., Han, B., Zhang, Y., and Chen, S. (2010). Mesozoic and Cenozoic Crust-Mantle Interaction in the Central Asian Orogenic Belt: A Comparative Study of Mantle-Derived Magmatic Rocks in Northern Xinjiang. *Acta Petrol. Sin.* 26, 431–439. [in Chinese with English Abstract].

Han, B.-F., He, G.-Q., Wang, X.-C., and Guo, Z.-J. (2011). Late Carboniferous Collision between the Tarim and Kazakhstan-Yili Terranes in the Western Segment of the South Tian Shan Orogen, Central Asia, and Implications for the Northern Xinjiang, Western China. *Earth-Sci. Rev.* 109, 74–93. doi:10.1016/j.earscirev.2011.09.001

He, D., Chen, X., Kuang, J., Zhou, L., Tang, Y., and Liu, D. (2008). Development and Genetic Mechanism of Chepaizi-Mosuowan Uplift in Junggar Basin, China. *Earth Sci. Front.* 15, 42–55. doi:10.1016/S1872-5791(08)60038-X

He, D., Zhang, L., and Wu, S. (2018). Tectonic Evolution Stages and Features of the Junggar Basin. *Oil Gas Geol.* 39, 845–861. [in Chinese with English abstract]. doi:10.11743/ogg20180501

Hendrix, M. S., Graham, S. A., Carroll, A. R., Sobel, E. R., McKNIGHT, C. L., Schulein, B. J., et al. (1992). Sedimentary Record and Climatic Implications of Recurrent Deformation in the Tian Shan: Evidence from Mesozoic Strata of the North Tarim, South Junggar, and Turpan Basins, Northwest China. *Geol. Soc. America Bull.* 104, 53–79. doi:10.1130/0016-7606(1992)104<0053:sracio>2.3.co;2

Hendrix, M. S. (2000). Evolution of Mesozoic sandstone Compositions, Southern Junggar, Northern Tarim, and Western Turpan Basins, Northwest China: A Detrital Record of the Ancestral Tian Shan. *J. Sediment. Res.* 70, 520–532. doi:10.1306/2DC40924-0E47-11D7-8643000102C1865D

Huang, D. (2019). Jurassic Integrative Stratigraphy and Timescale of China. *Sci. China Earth Sci.* 49, 227–256. [in Chinese with English abstract]. doi:10.1007/s11430-017-9268-7

Jackson, S. E., Pearson, N. J., Griffin, W. L., and Belousova, E. A. (2004). The Application of Laser Ablation-Inductively Coupled Plasma-Mass Spectrometry to *In Situ* U-Pb Zircon Geochronology. *Chem. Geol.* 211, 47–69. doi:10.1016/j.chemgeo.2004.06.017

Johnson, C. J., and Ritts, B. D. (2012). "Plate interior Polyphase Basins," in *Tectonics of Sedimentary Basins: Recent Advances*. Editors C. Busby and A. Azor (Wiley-Blackwell), 567–582. doi:10.1002/9781444347166.ch28

Jolivet, M., Bourquin, S., Heilbronn, G., Robin, C., Barrier, L., Dabard, M.-P., et al. (2017). The Upper Jurassic-Lower Cretaceous Alluvial-Fan Deposits of the Kalaza Formation (Central Asia): Tectonic Pulse or Increased Aridity? *Geol. Soc. Lond. Spec. Publ.* 427, 491–521. doi:10.1144/SP427.6

Kapp, P., Yin, A., Harrison, T. M., and Ding, L. (2005). Cretaceous-Tertiary Shortening, basin Development, and Volcanism in Central Tibet. *Geol. Soc. Am. Bull.* 117, 865–878. doi:10.1130/b25595.1

Li, S., Yu, X., Tan, C., and Steel, R. (2014). Jurassic Sedimentary Evolution of Southern Junggar Basin: Implication for Palaeoclimate Changes in Northern Xinjiang Uygur Autonomous Region, China. *J. Paleogeogr.* 3, 145–161. doi:10.3724/SP.J.1261.2014.00049

Li, Z., and Peng, S. (2013). U-Pb Geochronological Records and Provenance System Analysis of the Mesozoic-Cenozoic Sandstone Detrital Zircons in the Northern and Southern Piedmonts of Tianshan, Northwest China: Responses to Intracontinental Basin-Range Evolution. *Acta Petrol. Sin.* 29, 739–755.

Liu, S., Deng, B., Li, Z., and Sun, W. (2012). Architecture of basin-mountain Systems and Their Influences on Gas Distribution: A Case Study from the Sichuan Basin, South China. *J. Asian Earth Sci.* 47, 204–215. doi:10.1016/j.jseaes.2011.10.012

Liu, S., Dou, H., Zhang, W., Peng, Z., Zhang, L., and Zhang, W. (2018). Discovery of Jurassic Trachyandesite and its Geological Significance in the Northwestern of Junngar Basin. *Geol. Rev.* 64, 1519–1529. [in Chinese with English abstract]. doi:10.16509/j.georeview.2018.06.015

Liu, S., Dou, H., Li, H., and Wen, Z. (2019). Geological Significance of the Discovery of Late Jurassic Intermediate-Acidic Intrusive Rock in Bogeda Area of Eastern Tianshan, Xinjiang, and its U-Pb Zircon Age. *Geol. Bull. China* 38, 299–294. [in Chinese with English abstract].

Ludwig, K. R. (2003). *ISOPLOT 3: A Geochronological Toolkit for Microsoft Excel*. Berkeley: Berkeley Geochronology Centre Special Publication, 1–74.

Ma, L. F. (2002). *Geological Atlas of People's Republic of China*. Beijing: Chinese Map Publishing House. [in Chinese].

Mange, M. A., and Maurer, H. F. W. (2012). *Heavy Minerals in Colour*. Dordrecht: Springer Science and Business Media.

Morin, J., Jolivet, M., Robin, C., Heilbronn, G., Barrier, L., Bourquin, S., et al. (2018). Jurassic Paleogeography of the Tian Shan: An Evolution Driven by Far-Field Tectonics and Climate. *Earth-Sci. Rev.* 187, 286–313. doi:10.1016/j.earscirev.2018.10.007

Morin, J., Jolivet, M., Shaw, D., Bourquin, S., and Bataleva, E. (2021). New Sedimentological and Palynological Data from the Yarkand-Fergana Basin (Kyrgyz Tian Shan): Insights on its Mesozoic Paleogeographic and Tectonic Evolution. *Geosci. Front.* 12, 183–202. doi:10.1016/j.gsf.2020.04.010

Ni, M., Chen, S., Liu, Z., Shang, F., Qi, J., and Wang, L. (2019). Structural Evolution of Chepaizi Uplift and its Control on Stratigraphic Deposition in the Western Junggar Basin, China. *Acta Geol. Sin. - Eng. Ed.* 93 (4), 1060–1075. doi:10.1111/1755-6724.13854

Ritts, B. D., Weislogel, A., Graham, S. A., and Darby, B. J. (2009). Mesozoic Tectonics and Sedimentation of the Giant Polyphase Nonmarine Intraplate Ordos Basin, Western North China Block. *Int. Geol. Rev.* 51, 95–115. doi:10.1080/00206810802614523

Shen, C. B., Mei, L. F., Liu, L., Tang, J. G., and Zhou, F. (2006). Evidence from Apatite and Zircon Fission-Track Analysis for Mesozoic-Cenozoic Uplift thermal History of Bogda Mountain of Xinjiang, Northwest China. *Mar. Goel. Quat. Geol.* 26, 87–92.

Shen, C. B., Mei, L. F., Zhang, S. W., Liu, L., Tang, J. G., Zhou, F., et al. (2008). Fission-track Dating Evidence on Space-Time Difference of Mesozoic-Cenozoic Uplift of the Yilianhabierga Mountain and Bogda Mountain. *J. Mineralogy Petrol.* 28 (2), 63–70. [in Chinese with English Abstract]. doi:10.19719/j.cnki.1001-6872.2008.02.012

Tang, W., Zhang, Z., Li, J., Li, K., Chen, Y., and Guo, Z. (2014). Late Paleozoic to Jurassic Tectonic Evolution of the Bogda Area (Northwest China): Evidence from Detrital Zircon U-Pb Geochronology. *Tectonophysics* 626, 144–156. doi:10.1016/j.tecto.2014.04.005

Tang, W., Zhang, Z., Li, J., Li, K., Luo, Z., and Chen, Y. (2015). Mesozoic and Cenozoic Uplift and Exhumation of the Bogda Mountain, NW China: Evidence from Apatite Fission Track Analysis. *Geosci. Front.* 6, 617–625. doi:10.1016/j.gsf.2014.04.006

Tian, Y. (2017). *Study on Jurassic Palynological Assemblages and Paleoclimate of the Mid-western Area of the Junggar Basin*. Beijing: China University of Geosciences. [dissertation/master's thesis].

Torsvik, T. H., Van der Voo, R., Preeden, U., Mac Niocaill, C., Steinberger, B., Doubrovine, P. V., et al. (2012). Phanerozoic Polar Wander, Palaeogeography and Dynamics. *Earth-Sci. Rev.* 114, 325–368. doi:10.1016/j.earscirev.2012.06.007

Walsh, J. P., Wiberg, P. L., Aalto, R., Nittrouer, C. A., and Kuehl, S. A. (2016). Source-to-Sink Research: Economy of the Earth's Surface and its Strata. *Earth-Sci. Rev.* 153, 1–6. doi:10.1016/j.earscirev.2015.11.010

Wang, X., Wang, X., and Ma, Y. (2007). The Tectonic Evolution of Bogda Mountain, Xinjiang, Northwest China and its Relationship to Oil and Gas Accumulation. *Geoscience* 21 (1), 116.

Wang, J., Cao, Y. C., Wang, X. T., Liu, K. Y., Wang, Z. K., and Xu, Q. S. (2018). Sedimentological Constraints on the Initial Uplift of the West Bogda Mountains in Mid-permian. *Sci. Rep.* 8, 1453–1514. doi:10.1038/s41598-018-19856-3

Wang, Y., Jia, D., Pan, J., Wei, D., Tang, Y., Wang, G., et al. (2018). Multiple-phase Tectonic Superposition and Reworking in the Junggar Basin of Northwestern China-Implications for Deep-Seated Petroleum Exploration. *Bulletin* 102, 1489–1521. doi:10.1306/10181716518

Wei, P., Zhang, H., and Chen, Q. (2006). *Petroleum Geology and Exploration prospect in the Yingen–Ejinaqi Basin*. Beijing: Petroleum Industry Press.

Windley, B. F., Alexeiev, D., Xiao, W., Kröner, A., and Badarch, G. (2007). Tectonic Models for Accretion of the Central Asian Orogenic Belt. *J. Geol. Soc.* 164, 31–47. doi:10.1144/0016-76492006-022

Wu, C., Quan, S., Guo, Z., Qiu, R., Li, Y., Wang, Q., et al. (2004). The Prototypes Basins in Xinjiang, Western China. *Xinjiang Geology.* 22, 56–63. [in Chinese with English abstract]. doi:10.3969/j.issn.1000-8845.2004.01.010

Xiao, W., Windley, B. F., Allen, M. B., and Han, C. (2013). Paleozoic Multiple Accretionary and Collisional Tectonics of the Chinese Tianshan Orogenic Collage. *Gondwana Res.* 23, 1316–1341. doi:10.1016/j.gr.2012.01.012

Xu, X., Cheng, C., Ding, T., Liu, X., and Li, H. (2008). Discovery of Lisa basalt Northwestern Edge of Junggar Basin and its Geological Significance. *Xinjiang Geol.* 26, 9–16.

Yang, J., Xu, Z., Li, Z., Xu, X., Li, T., Ren, Y., et al. (2009). Discovery of an Eclogite belt in the Lhasa Block, Tibet: A New Border for Paleo-Tethys? *J. Asian Earth Sci.* 34, 76–89. doi:10.1016/j.jseaes.2008.04.001

Yang, W., Jolivet, M., Dupont-Nivet, G., Guo, Z., Zhang, Z., and Wu, C. (2013). Source to Sink Relations between the Tian Shan and Junggar Basin (Northwest China) from Late Palaeozoic to Quaternary: Evidence from Detrital U-Pb Zircon Geochronology. *Basin Res.* 25, 219–240. doi:10.1111/j.1365-2117.2012.00558.x

Yang, Y.-T., Song, C.-C., and He, S. (2015a). Jurassic Tectonostratigraphic Evolution of the Junggar Basin, NW China: A Record of Mesozoic Intraplate Deformation in Central Asia. *Tectonics* 34, 86–115. doi:10.1002/2014TC003640

Yang, Y.-T., Guo, Z.-X., Song, C.-C., Li, X.-B., and He, S. (2015b). A Short-Lived but Significant Mongol-Okhotsk Collisional Orogeny in Latest Jurassic-Earliest Cretaceous. *Gondwana Res.* 28, 1096–1116. doi:10.1016/j.gr.2014.09.010

Yi, Z., Liu, Y., and Meert, J. G. (2019). A True Polar Wander Trigger for the Great Jurassic East Asian Aridification. *Asian Aridification. Geol.* 47, 1112–1116. doi:10.1130/g46641.1

Yuan, M., Liang, S., Yan, L., Yan, Y., Tang, L., and Pang, X. (2002). *Oil & Gas Geology and Exploration Practice in the Turpan-Hami Basin*. Beijing: Petroleum Industry Press.

Yuan, H., Gao, S., Liu, X., Li, H., Günther, D., and Wu, F. (2004). Accurate U-Pb Age and Trace Element Determinations of Zircon by Laser Ablation-Inductively Coupled Plasma-Mass Spectrometry. *Geostand Geoanalyt Res.* 28, 353–370. doi:10.1111/j.1751-908x.2004.tb00755.x

Zhao, Y., Wei, D., Ma, Z., Yan, C., Liu, Y., Zhang, H., et al. (2003). *Jurassic System in the North of China (Vol. IV), Qilian Stratigraphic Region*. Beijing: Petroleum Industry Press.

Zhou, T., Wu, C., Yuan, B., Shi, Z., Wang, J., Zhu, W., et al. (2019). New Insights into Multiple Provenances Evolution of the Jurassic from Heavy Minerals Characteristics in Southern Junggar Basin, NW China. *Pet. Exploration Dev.* 46, 67–81. doi:10.1016/S1876-3804(19)30006-0

Zhou, T. (2020). *Effects of Sedimentary and Diagenetic Process on Pore Structure and Reservoir Quality in the Jurassic Tight sandstone Reservoirs of the Southern Junggar Basin, NW China*. Beijing: Peking Universiy. dissertation/doctor's thesis.

Zhu, W., Wu, C., Wang, J., Zhou, T., Li, J., Zhang, C., et al. (2017). Heavy mineral Compositions and Zircon U-Pb Ages of Cenozoic Sandstones in the SW Qaidam basin, Northern Tibetan Plateau: Implications for Provenance and Tectonic Setting. *J. Asian Earth Sci.* 146, 233–250. doi:10.1016/j.jseaes.2017.05.023

Zhu, W., Wang, F., Cao, Y., and Wang, S. (2020). Tectono-magmatic Events in Tianshan Mountains and Adjacent Areas during Yanshanian Movement Period. *Acta Geol. Sin.* 94, 1331–1346. [in Chinese with English abstract].

Conflict of Interest: Author XZ was employed by the company SINOPEC. Author WJ was employed by the company China National Nuclear Corporation.

The remaining authors declare that the research was conducted in the absence of any commercial or financial relation ships that could be construed as a potential conflict of interest.

Publisher's Note: All claims expressed in this article are solely those of the authors and do not necessarily represent those of their affiliated organizations, or those of the publisher, the editors and the reviewers. Any product that may be evaluated in this article, or claim that may be made by its manufacturer, is not guaranteed or endorsed by the publisher.